UNIVERSITE HASSIBA BENBOUALI DE CHLEF

Faculté de Technologie

Département d'Electronique

MEMOIRE DE MASTER

Domaine : SCIENCES ET TECHNOLOGIES

Filière : TELECOMMUNICATIONS

Spécialité : SYSTEMES DES TELECOMMUNICATIONS

Investigation and design of a high-speed optical system using millimeter waves

Par

M'HAMED SNOUSSI Assia

KOBZILI Hafsa

Encadreur :

Dr. ADARDOUR H. Errachid

Maître de Conférence « A » à l'UHBC

Co-Encadreur :

Pr. ALTUNCU Ahmet

Professeur à l'UAK-Turquie

Chlef, Juillet 2025

UNIVERSITE HASSIBA BENBOUALI DE CHLEF

Faculté de Technologie

Département d'Electronique

MEMOIRE DE MASTER

Domaine : SCIENCES ET TECHNOLOGIES

Filière : TELECOMMUNICATIONS

Spécialité : SYSTEMES DES TELECOMMUNICATIONS

Investigation and design of a high-speed optical system using millimeter waves

Par

M'HAMED SNOUSSI Assia

KOBZILI Hafsa

Encadreur :

Dr. ADARDOUR H. Errachid

Maître de Conférence « A » à l'UHBC

Co-Encadreur :

Pr. ALTUNCU Ahmet

Professeur à l'UAK-Turquie

Chlef, Juillet 2025

We dedicate this work to our beloved families, whose unconditional love, constant encouragement, and unwavering support have been the foundation of our perseverance and success.

To our dear friends, thank you for your companionship, encouragement, and understanding throughout this journey.

To Haroun Errachid ADARDOUR for his valuable advice, insightful comments, and continuous support, which have greatly enriched our work.

With our sincere thanks,

HAFSA & ASSIA

Acknowledgements

First of all, we thank Allah for the blessings of health and Islam, and for the assistance. He has granted us in accomplishing this work.

We would particularly like to express our sincere gratitude to Dr. Haroun Errachid ADARDOUR, Associate Professor "A" at Hassiba Benbouali University in Chlef, for his valuable guidance and continuous support throughout this work. His constructive criticism, insightful comments, and useful advice greatly contributed to the advancement of our research.

We also express our sincere gratitude to Prof. Ahmet ALTUNCU, Professor at Afyon Kocatepe University in Turkey, for agreeing to review, evaluate, and validate our work.

We also extend our sincere thanks to all the professors and teachers who have contributed to our education throughout our academic journey.

Finally, we hope that our parents, families, and friends find in these few lines a reflection of our deep appreciation for their constant support and encouragement. We thank you warmly.

Abstract Radio over Multi-Modes Fiber-Free Space Optics (RoMMF-FSO) represents a promising hybrid communication approach that merges the high bandwidth capabilities of optical wireless links with the adaptability of radio frequency technologies, such as MilliMeter Waves (MMWs). This study evaluates the performance of the proposed system using the RoMMF-FSO link under diverse Atmospheric Turbulence (AT) conditions, specifically weak, moderate, and strong, with different levels (light, medium, and heavy) of Weather Conditions (WCs) employing the OptiSystem simulation platform. However, different levels of weather-related attenuation are tested, and a wide range of transmission distances are applied to evaluate key performance metrics, including Bit Error Rate (BER), Quality Factor (Q-Factor), and Communication Capacity (CC). Another important part of the analysis is how increasing the transmitted optical power affects the stability and resilience of the system. The simulation of the obtained results shows that increasing the optical transmission power, especially in weak AT scenarios, significantly improves the proposed system's performance for longer transmission distances. Although, extreme WCs, such as dense fog and heavy rain, continue to degrade transmission quality. On the other hand, when using the moderate and strong ATs, the proposed system's performance operates with only lower optical transmission power for shorter transmission distances, given the same WCs, due to the higher frequencies within the MMW bands. These results confirm that RoMMF-FSO links are viable for future 5G wireless networks and beyond, especially for last-mile connectivity networks under adverse environmental conditions.

Keywords: RoMMF, FSO, atmospheric turbulence, weather conditions, BER, Q-Factor, CC, OptiSystem.

Résumé La radio sur fibre optique multimode et sur optique en espace libre (RoMMF-FSO) représente une approche de communication hybride prometteuse qui fusionne les capacités de large bande passante des liaisons optiques sans fil avec l'adaptabilité des technologies de radiofréquence, telles que les ondes millimétriques (MMW). Cette étude évalue les performances du système proposé en utilisant la liaison RoMMF-FSO dans diverses conditions de turbulence atmosphérique (AT), notamment faible, modérée et forte, avec différents niveaux (léger, moyen et lourd) de conditions météorologiques (WCs) en utilisant la plateforme de simulation OptiSystem. Cependant, différents niveaux d'atténuation liés aux conditions météorologiques sont testés et une large gamme de distances de transmission est appliquée pour évaluer les principales mesures de performance, notamment le taux d'erreur sur les bits (BER), le facteur de qualité (Q-Factor) et la capacité de communication (CC). Une

autre partie importante de l'analyse porte sur la manière dont l'augmentation de la puissance optique transmise affecte la stabilité et la résilience du système. La simulation des résultats obtenus montre que l'augmentation de la puissance de transmission optique, en particulier dans les scénarios d'AT faible, améliore considérablement les performances du système proposé pour les longues distances de transmission. Cependant, des conditions extrêmes, telles qu'un brouillard dense ou une forte pluie, continuent de dégrader la qualité de la transmission. En revanche, lors de l'utilisation des AT modérés et forts, les performances du système proposé fonctionnent avec une puissance de transmission optique plus faible pour des distances de transmission plus courtes, compte tenu des mêmes WC, en raison des fréquences plus élevées dans les bandes MMW. Ces résultats confirment que les liaisons RoMMF-FSO sont viables pour les futurs réseaux sans fil 5G et au-delà, en particulier pour les réseaux de connectivité du dernier kilomètre dans des conditions environnementales défavorables.

Mots-clés : RoMMF, FSO, turbulence atmosphérique, conditions météorologiques, BER, Q-Factor, CC, OptiSystem.

الملخص يمثل الاتصال اللاسلكي عبر الألياف متعددة الأنماط واللاسلكي عبر بصريات الفضاء الحر (RoMMF-FSO) نهجاً واعداً للاتصالات الهجينة يدمج بين قدرات النطاق الترددي العالي للوصلات اللاسلكية الضوئية مع قابلية تكييف تقنيات الترددات اللاسلكية، مثل الموجات المليمترية (MMWs). تقوم هذه الدراسة بتقييم أداء النظام المقترح باستخدام وصلة RoMMF-FSO في ظل ظروف الاضطرابات الجوية المتنوعة (AT)، وتحديداً الضعيفة والمعتدلة والقوية، مع مستويات مختلفة (خفيفة ومتوسطة وثقيلة) من الظروف الجوية (WCs) باستخدام منصة محاكاة OptiSystem. ومع ذلك، يتم اختبار مستويات مختلفة من التوهين المرتبط بالطقس، ويتم تطبيق مجموعة واسعة من مسافات الإرسال لتقييم مقاييس الأداء الرئيسية، بما في ذلك معدل الخطأ في البت (BER)، وعامل الجودة (Q-Factor)، وسعة الاتصال (CC). جزء مهم آخر من التحليل هو كيفية تأثير زيادة الطاقة الضوئية المرسلة على استقرار النظام ومرونته. تُظهر محاكاة النتائج التي تم الحصول عليها أن زيادة قدرة الإرسال الضوئي، خاصة في سيناريوهات AT الضعيفة، تحسن أداء النظام المقترح لمسافات الإرسال الأطول بشكل كبير. وعلى الرغم من ذلك، تستمر حالات الضغط الجوي الشديد، مثل الضباب الكثيف والأمطار الغزيرة، في تدهور جودة الإرسال. من ناحية أخرى، عند استخدام حالات الضغط الجوي AT المعتدل والقوي، فإن أداء النظام المقترح يعمل بقدرة إرسال ضوئية أقل فقط لمسافات الإرسال الأقصر، بالنظر إلى نفس الضغط الجوي، وذلك بسبب الترددات الأعلى ضمن نطاقات الترددات الموجات المليمترية. تؤكد هذه النتائج أن وصلات RoMMF-FSO قابلة للتطبيق لشبكات الجيل الخامس اللاسلكية المستقبلية وما بعدها، خاصة لشبكات الاتصال في الميل الأخير في ظل الظروف البيئية المعاكسة.

الكلمات المفتاحية : RoMMF، FSO، الاضطرابات الغلاف الجوي، الظروف الجوية، معدل الخطأ في البت (BER)، عامل الجودة (Q-Factor)، سعة الاتصال (CC)، وOptiSystem.

Table of contents

Chapter 2 : Fundamental optoelectronic components for RoF and RoFSO links

Chapter 3: Study and evaluation of a 5G MMW transmission system using RoMMF-FSO for a 5GBUN

Abbreviation

4G: Fourth-**G**eneration

5G: Fifth-**G**eneration

5GNs: 5G Networks

5GBUN: 5G Back-**U**p **N**etwork

A

AA: Atmospheric **A**ttenuation

AM: Amplitude **M**odulator

APD: Avalanche **P**hoto-**D**iode

AT: Atmospheric **T**urbulence

B

BER: Bit **E**rror **R**ate

BS: Base **S**tation

C

CBS: Central **B**ase **S**tation

CC: Communication **C**apacity

CD: Chromatic **D**ispersion

CDMA: Code **D**ivision **M**ultiple **A**ccess

CS: Central **S**ite

CWL: Continuous **W**ave **L**aser

D

DML: Direct **M**odulation **L**aser

DTNCC: Data **T**ransmission and **N**etwork **C**ontrol **C**enter

E

EA: Electro-**A**bsorption

EAM: Electro-**A**bsorption **M**odulator

ECA: Electrical **C**arrier **A**nalyzer

EDFA: Erbium-**D**oped **F**iber **A**mplifier

EMI: Electro**M**agnetic **I**nterference

ESNR: Electrical **S**ignal-to-**N**oise **R**atio

F

FCC: Federal **C**ommunications **C**ommission

FMF: Few-**M**ode **F**ibers

FRA: Fiber **R**aman **A**mplifiers

FSO: Free **S**pace **O**ptical

G

GaAsP: Gallium **A**rsenide **P**hosphide

Gbps: Giga **b**its **p**er **s**econd

GG: Gamma-**G**amma

GGD: GG Distribution

H

HD: High **D**efinition

HSWC: High-**S**peed **W**ireless **C**ommunications

I

IEEE: Institute of **E**lectrical and **E**lectronics **E**ngineers

IF: Intermediate **F**requency

K

Ka-band: Kurtz-**a**bove **band**

L

LAN: Local **A**rea **N**etworks

LD: Laser **D**iode

LED: Light **E**mitting **D**iode

LG: Laguerre-**G**auss

LoS: Line **o**f **S**ight

LO: Local **O**scillator

LPF: Low-**P**ass **F**ilter

LTM-G: Laguerre **T**ransverse **M**ode **G**enerator

M

MCF: **M**ulti-**C**ore Multiplexing

MD: Multimode **D**ispersion

MDM: Mode **D**ivision **M**ultiplexing

MHz: Miga **H**ert**z**

MIMO: Multiple-**I**nput **M**ultiple-**O**utput

MMF: Multi-**M**ode **F**ibers

MMW: Milli**M**eter-**W**ave

MS: Mode **S**elector

MZM: Mach-**Z**ehnder **M**odulator

N

NLoS: Non-Line **o**f **S**ight

NRZP-G: Non-**R**eturn-to-**Z**ero **P**ulse **G**enerator

O

OF: Optical **F**iber

OFDM: Orthogonal **F**requency **D**ivision **M**ultiplexing

OPLL: Optical **P**hase **L**ocked **L**oop

P

PC: Power **C**ombiner

PD: Photo**d**iode

PDF: Probability **D**ensity **F**unction

PIMF: Parabolic **I**ndex **M**ultimode **F**iber

PIN-PD: Positive-**I**ntrinsic-**N**egative **P**hotodiode

PMD: Polarization **M**ode **D**ispersion

PN: Pseudo-**N**oise

PNJ: Positive **N**egative **J**unction

PRBS-G: Pseudo-**R**andom **B**inary **S**equence **G**enerator

PS: Power **S**plitter

Q

Q-Factor: **Q**uality-**Factor**

R

RAU: Remote **A**ntenna **U**nit

RBS: Remote **B**ase **S**tation

RF: Radio **F**requency

RoF: Radio **o**ver **F**iber

RoFSO: Radio **o**ver **F**ree **S**pace **O**ptical

RoF-FSO: Radio **o**ver **F**iber-**F**ree **S**pace **O**ptical

RoMMF-FSO: Radio **o**ver **M**ulti**M**ode **F**iber-**F**ree **S**pace **O**ptical

ROPB: Received **O**ptical **P**ower **B**eam

Rx: Receiver **x**

S

SDM: Spatial **D**ivision **M**ultiplexing

SMF: Single-**M**ode **F**ibers

SNR: Signal-to-**N**oise **R**atio

SOA: Semiconductor **O**ptical **A**mplifier

SSB: Single **S**ide**B**and

T

Tbps: Tera **b**its **p**er **s**econd

THz: Tera **H**ert**z**

TV: Tele**V**ision

Tx: Transmitter **x**

U

UAV: Unmanned **A**erial **V**ehicles

UMTS: Universal **M**obile **T**elecommunications **S**ystem

W

WAN: Wide **A**rea **N**etworks

WC: Weather **C**onditions

WLANs: Wireless **L**ocal **A**rea **N**etworks

WDM: Wavelength **D**ivision **M**ultiplexing

List of Figures

Chapter 1

Chapter 2

Chapter 3

List of Tables

Chapter 3

General introduction

In modern wireless networks, such as 5G transmission, the increasing demand for high-speed, low-latency, and reliable communication has led to the development of hybrid technologies that manage these challenges. One such promising solution is the integration of Radio over MultiMode Fiber (RoMMF) and Free-Space Optics (FSO), resulting in a RoMMF-FSO system. This type of hybrid architecture leverages the high bandwidth and low transmission loss of free-space optical wireless links while also benefiting from their deployment flexibility and cost-effectiveness.

FSO technology provides a high-capacity, license-free communication channel that is resistant to electromagnetic interference. However, its performance is significantly impaired by atmospheric conditions such as fog, rain, snow, and dust, which cause severe signal attenuation and distortion. In contrast, RoMMF systems enable the transmission of high-frequency radio signals over optical fibers, which promotes centralized processing and simplifies the design of remote antenna devices.

By integrating RoMMF and FSO, this hybrid method shows substantial advantages for next-generation wireless systems (i.e., Future Communication Networks (FCNs)), especially for access to the last kilometer in densely populated or urban areas. As such, it is an exceptional candidate for 5G deployment and FCNs that require high data rates and flexible infrastructure. However, to ensure reliable performance under varying weather conditions, system behavior must be thoroughly evaluated.

This work concentrates on the simulation and performance analysis of the transmitted multi-beam MilliMeter Wave (MMW) signals over RoMMF-FSO (Radio over MultiMode Fiber-Free Space Optical) communication system using the SDM (Space-Division Multiplexing) technique in various atmospheric scenarios employing OptiSystem software. The main performance metrics of the proposed system, namely Bit Error Rate (BER), Quality-Factor (Q-Factor), and Communication Capacity (CC), are examined over different distances of the FSO link under weather conditions. The objective is to evaluate the impact of environmental factors and propose optimized parameters to improve the robustness and efficiency of the proposed system.

The structure of the work is as follows:

Chapter 1 presents the application of millimeter waves in RoF and FSO systems, examining their characteristics, advantages, challenges, and potential use cases.

Chapter 2 provides an overview of the main optoelectronic components used in RoF and FSO systems.

Chapter 3 presents detailed simulation results on the performance of RoMMF-FSO links under different weather conditions using OptiSystem. It includes an evaluation of the system's capability to distribute MMW signals to four remote receivers through an FSO link, analyzing indicators such as, BER, Q-Factor and CC to judge the performance of the proposed system. The paper concludes with a general summary and final thoughts.

CHAPTER 1

Millimeter waves in OF and FSO technologies

1.1. Introduction

In High-Speed Wireless Communications (HSWC), MilliMeter-Wave (MMW) technology has garnered considerable attention. MMW frequencies [30–300 GHz] present a good reaction to the rising demand for more rapid data rates and more bandwidth. This chapter investigates the potential of MMW technology in HSWC, with a focus on its applications in radio transmission over Optical Fiber (OF) and free space [1-3].

1.2. Millimeter-waves

MMW technology is the application of electromagnetic waves with wavelengths between [30 and 300 GHz] corresponding to [1 to 10 mm] (see Figure 1.1). These high-frequency waves enable HSWC, making them a key component of 5G Networks (5GNs), satellite communications, and radar systems [4,5].

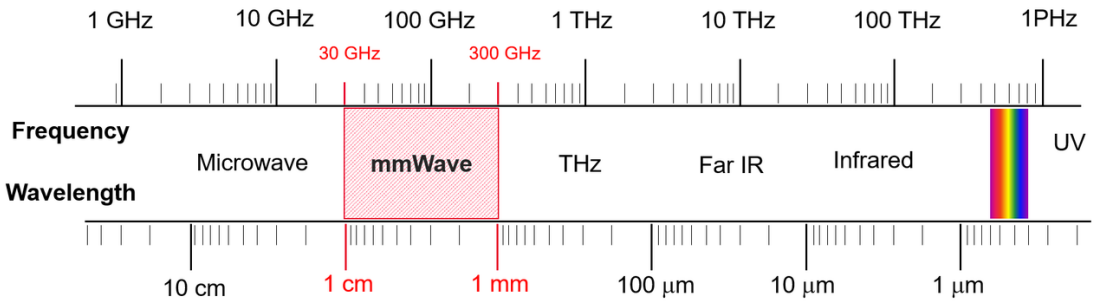

Figure 1.1. MMW frequencies bands [5].

1.2.1. Properties and characteristics of MMW

MWW communication has several key characteristics. These include high propagation loss, short wavelengths, and wide bandwidth. A summary of these notable features is presented below [6]:

- The high data rates provided by MMW communication exceed those of conventional microwaves.
- MMW signals allow large-scale MIMO (Multiple-Input Multiple-Output) systems for optimal spectral efficiency.
- High frequencies result in higher propagation loss; however, high-gain directional antennas can mitigate this effect.
- High frequencies in Non-Line-of-Sight (NLoS) situations make it challenging to cover indoor areas with outdoor MMW nodes.

1.2.2. Challenges in 5G MMW technology

5GNs rely on MMW technology, which promises more rapid data transfer and more significant bandwidth than conventional microwave technology. Nonetheless, their deployment is problematized by characteristics such as signal blocking, atmospheric absorption, and path loss. Here, we give a quick overview of a few of these issues [7,8]:

- High-frequency signals generate significant free-space path loss, weakening the signal over long distances.
- In situations where there is NLoS, the effectiveness of MMWs is limited by obstacles such as people, trees, and buildings.
- Signal throughput is significantly affected by attenuation from atmospheric oxygen.
- The high cost of components is attributed to the use of specialized parts and materials.
- The high level of precision required for connector alignment poses manufacturing and assembly challenges.
- Testing and debugging problems require specialized and expensive equipment.

1.2.3. Advantages of MMW

Internet gaming and HD (High Definition) video streaming platforms are two applications that utilize a significant amount of bandwidth from MMW technology, which can deliver data rates exceeding 10 Gbps or more. In addition, the enhancement of resolution and the narrow beam approach of 5G antennas make them ideal for high-precision imaging and transmission. Further, made feasible by the small component size are functional and straightforward antenna configurations. Furthermore, their limited range and narrow beam help improve communication privacy by reducing signal interception and thereby increasing security [9].

1.2.4. Applications of MMW technology

Telecommunications, automotive radar, imaging, security, healthcare, industrial sectors, and scientific research are just a few of the many uses for MMW technology, which operates in the [30 GHz to 300 GHz] range (see Figure 1.2). Wireless standards like multi-gigabit wireless systems (IEEE 802.11ad) and 5G cellular networks, which operate between [24 GHz and 39 GHz], are among the main applications. Additionally, radar systems feature 95 GHz fire control and Ka-band speed detection. Further, medical systems employing therapy to treat illnesses operate within the frequency range of 40 GHz to 70 GHz. Furthermore, industrial systems are used to measure thickness in the manufacturing of glass, plastic, and paper.

Ultimately, scientific investigations, such as radio astronomy and remote sensing, are used [10].

Figure 1.2. MMW applications [9].

1.3. Radio over fiber

To enable wireless access and transmission, a technology known as Radio over Fiber (RoF) modulates light employing Radio Frequency (RF) signals and transmits it through OF. Broadband access systems, cellular networks, and wireless communication all employ it extensively [11-13].

1.3.1. Basic architecture of RoF system

Figure 1.3 depicts a simple RoF system. The Central Site (CS) is responsible for generating RF signals and modulating them onto an optical carrier using a Laser Diode (LD) in downlink transmission. In addition, these modulated optical signals are then transmitted through an OF link to the Base Station (BS) or Remote Antenna Unit (RAU). Furthermore, the optical signal is converted by a Photo-Detector (PD) at the BS, amplified, and transmitted through an RF antenna. However, for uplink transmission, a LD converts the received RF signals at the RF antenna into optical signals, which are then transmitted back to the CS through the OF [14-16].

1.3.2. Advantages of RoF

RoF technology offers several advantages, including low attenuation loss, high bandwidth capacity, immunity to electromagnetic interference, ease of installation and maintenance, multi-operator and multi-service support, dynamic resource allocation, and low power consumption. It also provides cost-effective solutions for the long-distance transmission of high-frequency signals, optimizing network efficiency and coverage [17-21].

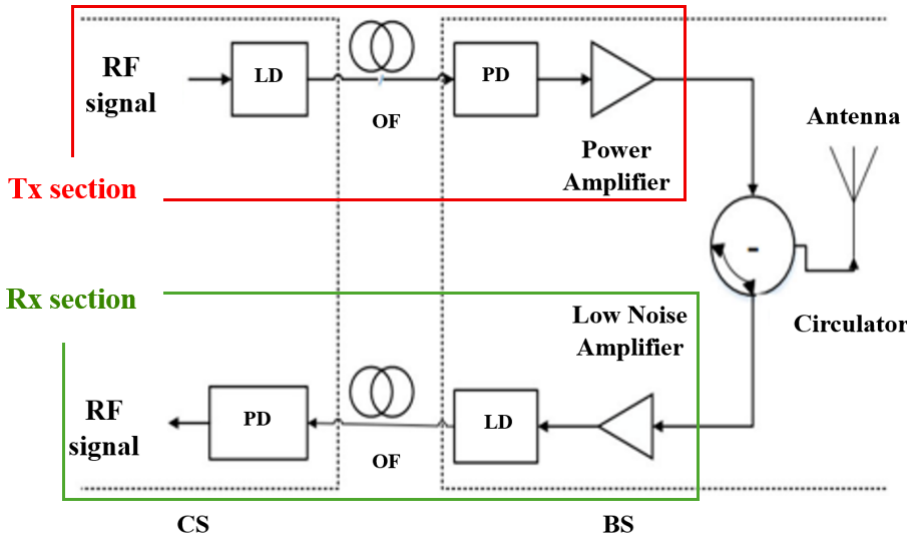

Figure 1.3. RoF system architecture [14-16].

1.3.3. Applications of RoF

The RoF system includes numerous applications, including enhancing cable TV networks and satellite control, improving mobile networks, enabling vehicle-to-vehicle communication, supporting next-generation Wireless Local Area Networks (WLANs), and providing mobile broadband services with increased bandwidth. It also enhances video distribution systems and satellite control, and it is compatible with Universal Mobile Telecommunications System (UMTS), 4G, and other emerging technologies [22-27].

1.3.4. Challenges and solutions implementing RoF

The optical-wireless systems face multiple significant technical challenges. Direct modulation is restricted for modulation at MMW frequencies, so external modulation, optical heterodyne, or Electro-Absorption (EA) modulators are required. SSB (Single SideBand) modulation or photonic down-conversion can make up for chromatic dispersion in fibers. Cancellation methods, sideband injection locking, corrective coding, or Optical Phase-Locked Loops (OPLL) can support and reduce phase distortions (phase noise). Pre- or post-distortion strategies are recommended to deal with laser/fiber nonlinearities.

In addition, a characterization that links optical properties and wireless noise addresses the noise specific to these links. Using PN (Pseudo-Noise) codes for multi-user detection in nonlinear environments enables the detection of correlations. Centralizing processing at the Central BS (CBS) makes Remote BS (RBS) more straightforward and more cost-effective. This is because it eliminates the laser, electrical mixer, and power supply in the RBS.

Furthermore, the optical down-conversion and electrical processing in the IF (Intermediate Frequency) make the expensive uplink operate better. Smart antennas and new technologies like MIMO-OFDM-CDMA are required for high data rate communication links that collaborate effectively together. Customers want smaller sizes and more affordable options, as there are few affordable optical-electronic interfaces on the market.

Finally, the hardware problems (modulation, dispersion, noise), complicated architecture (RBS, uplink), and fast integration are some of the biggest problems. The suggested solutions use new optical technologies (SSB, OPLL), improve the system (by centralizing it or removing components), and use more advanced methods (MIMO-OFDM-CDMA, IF processing). Researchers are still working on ways to cut costs and make interfaces smaller [27-30].

1.4. Radio over Free Space Optical (RoFSO)

RoFSO is the sending of RF signals through an open environment, like air, a vacuum, or outer space, without using cables or waveguides to carry the signals. It is the foundation of wireless communication systems like broadcasting, satellite communication, radar, and mobile networks [31].

1.4.1. Design and architecture of RoFSO system

Several key elements make up the architecture of a RoFSO communication system, see Figure 1.4. These elements work together to rapidly transfer data across an open space (FSO). The first step is to modulate the RF data signals, which transmit the information. Then, optical modulation, typically performed using a laser or LED, transforms these modulated radio frequency signals into optical signals. Transmitter optics (Tx optics) concentrate and transmit the light beam to the receiver.

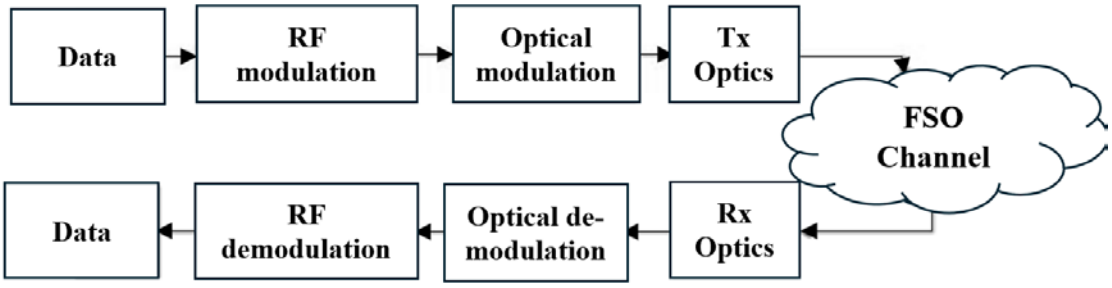

Figure 1.4. A RoFSO communication system's basic architecture [32-34].

A clear line of sight (LoS) between the transmitter and receiver is essential for optical signals to pass via the FSO channel. The receiver optics (Rx optics) on the other end pick up the optical signals and concentrate the incoming light onto a photodetector. The received optical signals are then converted back into electrical (RF) signals through optical demodulation. The data RF demodulation step takes the RF signals and breaks them down so that the original data can be recovered [32-34].

1.4.2. FSO's advantages for optical communication

FSO has a lot of advantages besides its large bandwidth. It works in the THz band, which is an unregulated range. This means it doesn't have to worry about FCC (Federal Communications Commission) licensing issues or interference. It also costs less than fiber optics or leased lines, and you don't have to put a lot of money into it right away. Deployment is quick and can be done in just a few days or weeks, so there is no need for permits or digging. The network architecture is flexible, and adding nodes to it is easy and doesn't require major changes. Open interfaces make the solution scalable and work with many providers, which protects investments in infrastructure. Lastly, it's very safe because its beams are hard to see, point in a certain direction, and are very thin, making them hard to catch. Encryption also makes it even harder to protect data [35].

1.4.3. Problems and limits of FSO

Several issues with FSO communication can make it less reliable and less effective, see Figure 1.5. Fog and bad weather are two of the most significant problems because they significantly weaken optical signals. Further, scintillation from atmospheric turbulence causes optical signals to fluctuate, increasing the number of errors. Wind and temperature changes in winter can cause the transmitter (Tx optic) and receiver (Rx optic) to become out of alignment, and the building's sway can further destabilize the pointing. High-power laser beams can also be dangerous for the eyes, and there is a risk of optical signal blocking or

jamming. FSO is also only suitable for short to medium distances unless relay stations are used. Strong sunlight can also cause noise and reduce the effectiveness of optical receivers by interfering with them [36].

1.4.4. FSO applications

FSO technology is now used in multiple locations for different services. Some of its uses have been to provide outdoor wireless access for carriers without requiring spectrum licenses and to offer last-mile coverage as a more cost-effective alternative to fiber optics. It enables the connection of LANs between business buildings and serves as a backup link for broken fiber optic cables. FSO also expands metropolitan area networks by linking new infrastructure to the core network. It is also the backbone for Wide Area Network (WAN) access, which is used by mobile users and satellite terminals. It lets people talk to each other one-on-one or in groups, even if they're in different buildings, ships, planes, or satellites. Lastly, its quick setup and built-in security make it great for military communications that can't be seen [37].

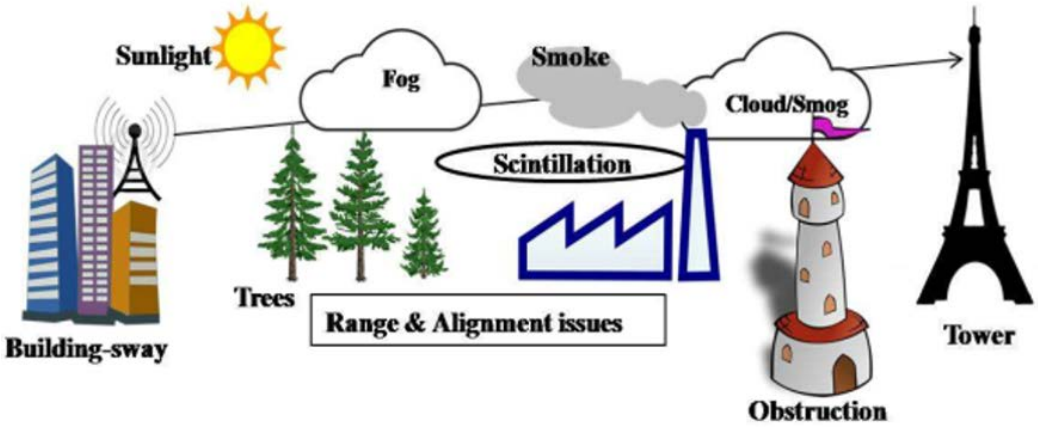

Figure 1.5. Problems and limits of FSO [36].

1.5. Conclusion

This chapter discusses the importance of MMW technology, RoF, and RoFSO for modern optical communication, especially in the context of 5G. The next chapter will discuss the basic optoelectronic components that enable the building of high-speed optical systems using MMW technology.

1.6. References of chapter 1

1. Wang, K., Lam, C. T., & Ng, B. K. (2022). Positioning information based high-speed communications with multiple RISs: Doppler mitigation and hardware impairments. *Applied Sciences*, *12*(14), 7076.

2. Elalaouy, O., Ghzaoui, M. E., & Foshi, J. (2024). A high-isolated wideband two-port MIMO antenna for 5G millimeter-wave applications. Results in Engineering, 23, 102466.
3. Wang, R., Yang, Y., Makki, B., & Shamim, A. (2024). A wideband reconfigurable intelligent surface for 5G millimeter-wave applications. IEEE transactions on antennas and propagation, 72(3), 2399-2410.
4. Rappaport, T. S., Xing, Y., Kanhere, O., Ju, S., Madanayake, A., Mandal, S., ... & Trichopoulos, G. C. (2019). Wireless communications and applications above 100 GHz: Opportunities and challenges for 6G and beyond. *IEEE access*, *7*, 78729-78757.
5. https://wiki.dfrobot.com/What_is_mmWave_Millimeter_Wave. Accessed 05/31/2025 at 11:58 p.m.
6. Lin, Z., Du, X., Chen, H. H., Ai, B., Chen, Z., & Wu, D. (2019). Millimeter-wave propagation modeling and measurements for 5G mobile networks. *IEEE Wireless Communications*, *26*(1), 72-77.
7. Al-Ogaili, F., & Shubair, R. M. (2016, June). Millimeter-wave mobile communications for 5G: Challenges and opportunities. In *2016 IEEE International Symposium on Antennas and Propagation (APSURSI)* (pp. 1003-1004). IEEE.
8. https://www.5gtechnologyworld.com/mmwaves-bring-interconnect-challenges-to-5g-and-6g. Accessed 06/01/2025 at 10:53 p.m.
9. Chittimoju, G., & Yalavarthi, U. D. (2021, February). A comprehensive review on millimeter waves applications and antennas. In Journal of Physics: Conference Series (Vol. 1804, No. 1, p. 012205). IOP Publishing.
10. Ashraf, S., Sheikh, J. A., Ashraf, A., & Rasool, U. (2024). 5g millimeter wave technology: An overview. Intelligent Signal Processing and RF Energy Harvesting for State of art 5G and B5G Networks, 97-112.
11. Mohan, A., & Anisha, A. P. (2015). Full duplex transmission in RoF system using WDM and OADM technology. *International Journal of Engineering Research & Technology (IJERT)*, *4*(1), 513-516.
12. Kanesan, T., Ng, W. P., Ghassemlooy, Z., & Lu, C. (2013). Experimental full duplex simultaneous transmission of LTE over a DWDM directly modulated RoF system. *Journal of optical Communications and Networking*, *6*(1), 8-17.
13. Dar, A. B., & Ahmad, F. (2019). A full-duplex 40 GHz radio-over-fiber transmission system based on frequency octupling. *Optical and quantum electronics*, *51*, 1-11.
14. Sumedha, P., Amitabh, A., & Mishra, S. (2015). Radio over Fiber (RoF) Technology. *International Journal of Research in Advent Technology*, *3*(9), 53-57.

15. Khalil, H., Qamar, F., Shahzadi, R., Shahzad, A., Ali, M., Qamar, N., & Al-Otaibi, S. (2021). Performance analysis of modulation formats for next generation RoF systems. IEEE Access, 9, 139393-139402.
16. Yücel, M., & Açikgöz, M. (2023). Optical communication infrastructure in new generation mobile networks. *Fiber and Integrated Optics*, *42*(2), 53-92.
17. Pooja, M., Saroj, S., & Manisha, B. (2015). Advantages and limitations of radio over fiber system. *International Journal of Computer Science and Mobile Computing*, *4*(5), 506-511.
18. Singh, R., Ahlawat, M., & Sharma, D. (2017). A review on radio over fiber communication system. *International Journal of Enhanced Research in Management & Computer Applications*, *6*(4), 23-29.
19. Rajpal, S., & Goyal, R. (2017). A review on radio-over-fiber technology-based integrated (optical/wireless) networks. Journal of Optical Communications, 38(1), 19-25.
20. Kaur, B., & Sharma, N. (2022). Radio over Fiber (RoF) for future generation networks. In Broadband Connectivity in 5G and Beyond: Next Generation Networks (pp. 161-184). Cham: Springer International Publishing.
21. Fan, S., Cao, C., Zeng, X., Ning, J., Yan, X., Wang, R., ... & Wang, T. (2019). A RoF system based on polarization multiplexing and carrier suppression to generate frequency eightfold millimeter-wave. Results in Physics, 12, 1450-1454.
22. Thakur, P., & Bharti, M. (2025, February). Design and Performance Analysis of a 16-Channel DWDM RoF System Using 112 Gbps Coherent DP-QPSK Modulation. In 2025 10th International Conference on Signal Processing and Communication (ICSC) (pp. 65-69). IEEE.
23. Saiyyed, R., Sindhwani, M., Sachdeva, S., Pahuja, H., & Shukla, M. K. (2024). Optoelectronic equipment-based fault monitoring with 64QAM-OFDM RoF transmission. Journal of Optics, 1-12.
24. Mohammed, S., & Desher, I. (2025). WDM-RoF Architecture for Low-Cost and Large-Coverage 5G Applications. Engineering, Technology & Applied Science Research, 15(2), 21746-21753.
25. Tyagi, S. K., Mittal, P., & Kumar, P. (2022, November). A review on optical modulators used in radio over fiber (RoF) system for 6G IoT applications. In 2022 3rd International Conference on Issues and Challenges in Intelligent Computing Techniques (ICICT) (pp. 1-6). IEEE.

26. Seal, A., Bhutani, S., & Sangeetha, A. (2017, April). Performance analysis of radio over fiber (RoF) system for indoor applications. In 2017 international conference on technical advancements in computers and communications (ICTACC) (pp. 73-76). IEEE.
27. Singh, B., & Singh, D. (2016). A review on advantages and applications of radio over fiber system. *International Journal of Current Engineering and Technology*, *6*(3), 1042-1044.
28. Braun, R. P., Grosskopf, G., & Rohde, D. (1995, May). Optical millimeter-wave generation and transmission technologies for mobile communications, an overview. In IEEE NTC, Conference Proceedings Microwave Systems Conference (pp. 239-242). IEEE.
29. Noel, L., Wake, D., Moodie, D. G., Marcenac, D. D., Westbrook, L. D., & Nesset, D. (1997). Novel techniques for high-capacity 60-GHz fiber-radio transmission systems. IEEE transactions on microwave theory and techniques, 45(8), 1416-1423.
30. Abdolee, R., Ngah, R., Vakilian, V., & Rahman, T. A. (2007, December). Application of radio-over-fiber (ROF) in mobile communication. In 2007 Asia-Pacific Conference on Applied Electromagnetics (pp. 1-5). IEEE.
31. Henniger, H., & Wilfert, O. (2010). An introduction to free-space optical communications. *Radioengineering*, *19*(2), 203-212.
32. Jose, T., Narain Ponraj, D., & Victor Du John, H. (2021). Performance Analysis of a RoFSO Link for 5G Networks Under Adverse Weather Conditions. *Przeglad Elektrotechniczny*, *97*(4).
33. Derouiche, S., Kameche, S., & Adardour, H. E. (2025). Design and simulation of a secure MIMO-RoFSO communication system at 60 GHz relying on a chaotic optical signal. Journal of Optics, 1-17.
34. Mohammed, T. J., & Ali, M. A. A. (2025). Performance analysis of the RoFSO system over a log-normal turbulent link. Journal of Optical Communications, 45(s1), s2543-s2552.
35. Sadiku, M. N., Musa, S. M., & Nelatury, S. R. (2016). Free space optical communications: an overview. *European scientific journal*, *12*(9), 55-68.
36. Kumar, S., & Sharma, N. (2022). Emerging military applications of free space optical communication technology: A detailed review. In Journal of Physics: Conference Series (Vol. 2161, No. 1, p. 012011). IOP Publishing.
37. Malik, A., & Singh, P. (2015). Free space optics: current applications and future challenges. International journal of optics, 2015(1), 945483.

CHAPTER 2

Fundamental optoelectronic components for RoF and RoFSO links

2.1. Introduction

RoFSO and RoF technologies are gaining significant attention in modern communication systems due to their speed, low latency, and cost-effectiveness. RoFSO uses radio signals and transmits them through the atmosphere employing light, whereas RoF combines radio signals with OF networks [1,2]. This chapter discusses the primary optoelectronic components employed in these systems, including transmitters, receivers, amplifiers, and multiplexing techniques, as well as the challenges that arise when using them.

2.2. Optoelectronic transmitter

Optoelectronic transmitters are crucial for RoFSO and RoF communications because they convert electrical signals into optical signals that can be transmitted over wires or wirelessly. Light Emitting Diodes (LEDs) or Laser Diodes (LDs) are often used in these transmitters. LDs are better than LEDs because they are more coherent and direct. There are several key components, including a modulation unit that encodes data, a driver circuit that controls the LD, and a transmitting telescope that focuses the beam for RoFSO [3,4].

2.2.1. LEDs and LDs sources for RoF and RoFSO systems

The LED is a semiconductor diode that is made in a way and from a material that lets light through when an electric current flows through it. GaAsP (Gallium Arsenide Phosphide) is the most common semiconductor used to make red LEDs. When the positive and negative carriers meet at the diode's PN Junction (PNJ), they release light. The diode is built so that the light that comes from the junction can get out and be seen. The light that comes from this type of junction has a narrow spectral bandwidth, which gives it a certain color. This range of frequencies has to do with the energy band gap (ΔE_g) of the carriers in the junction. As shown in Figure 2.1, an LED is made up of a chip of semiconducting material that has been doped with impurities to make a PNJ. The source of the excitation voltage is V_{ex} [5].

However, An LD, or injection LD, is a device that uses the P-N junction of a diode as a lasing medium. The biasing of the LD, which is similar to that of an LED, gives it power. The LED usually gives out of incoherent light, while the LD gives out of coherent light. The basic design of an LD is shown in Figure 2.2 [6].

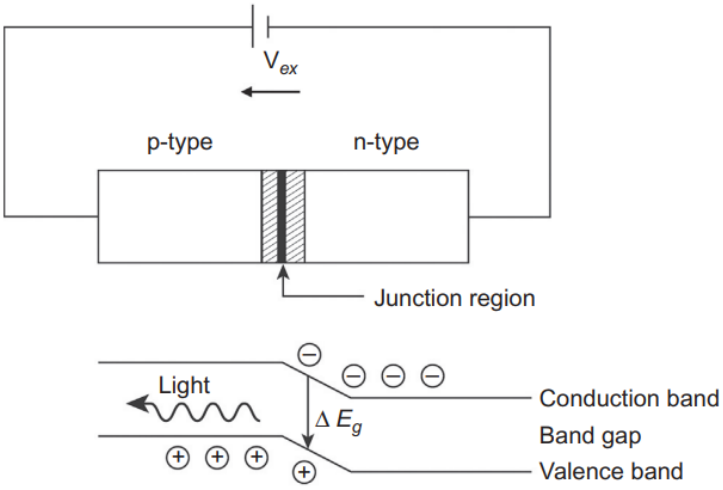

Figure 2.1. LED setup and energy bands [5].

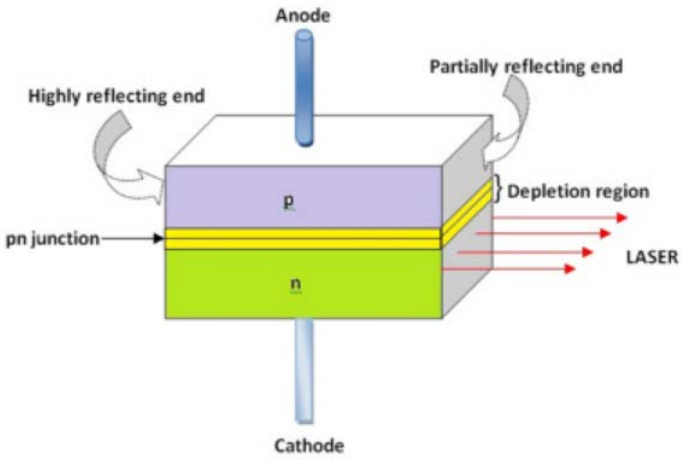

Figure 2.2. Design of LD [6].

2.2.2. LDs and LEDs

The OF or FSO communication systems primarily use two types of light sources. LDs operate by stimulated emission, which allows them to achieve high optical powers (up to 100 mW) and exhibit low angular dispersion. This latter characteristic facilitates their coupling with single-mode OFs. They are, therefore, preferred for high-speed communications (up to 10 Gbps) and over long distances. Conversely, LEDs emit light by spontaneous emission. A wide spectral width and lower optical power distinguish them. These properties make them primarily suitable for short-distance transmission applications, typically in conjunction with multimode OFs [7].

2.2.3. Optical modulators

Optical modulators (see Figure 2.3) are essential components in RoF and RoFSO systems, converting data into an optical signal. First, an external device called a Mach-Zehnder Modulator (MZM) uses optical interference to adjust the light intensity. This provides a wide bandwidth and improved signal integrity. Additionally, MZMs are ideal for long-distance transmissions because they do not introduce interference or parasitic frequency variations, unlike direct modulation solutions. However, MZM uses more power and, therefore, costs more [8,9].

The Electro-Absorbing Modulator (EAM) also leverages the electro-absorbing effect, which alters the light absorption by modifying the band gap of a semiconductor with an electric field. It has high data rates and moderate chirp but lower linearity. It is smaller and uses less energy than the MZM. EAM is often used as an alternative to other methods for applications that are located in the middle of the distance (metropolitan applications) [8,9].

A Direct Modulation Laser (DML) directly modulates the injection current of a laser. This makes it a cost-effective way to connect short distances (such as LAN applications). On the other hand, this technique, generates distortions in optical pulses, a narrow bandwidth, and a loud chirp, which deteriorates the signal quality over long distances [8,9].

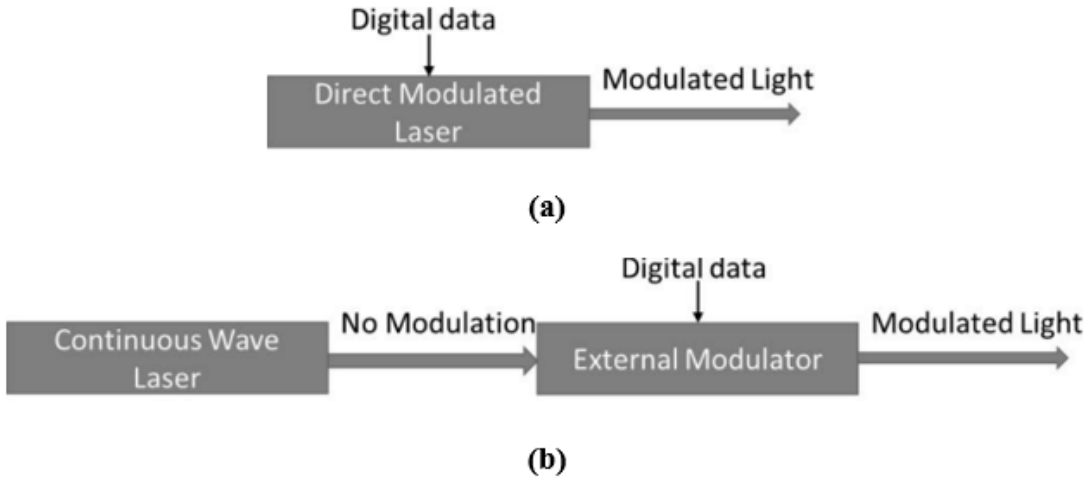

Figure 2.3. Direct modulation and external modulators are the two types of modulation schemes [8,9].

2.3. Channel

A transmission channel is a physical link that lets a transmitter send data to a receiver. It can encompass various types of media, such as coaxial cables, optical fibers, or free space for

wireless communication. Sending information through this channel can be hard because of noise and distortions that are part of the channel itself [10,11].

2.3.1. Integration of FSO and RoF systems in modern network

High-speed connectivity is significantly improved by combining the flexibility of FSO with the reliability of OF. Despite FSO technology's large bandwidth, signal quality can be affected by weather conditions. Wavelength Division Multiplexing (WDM) and enhanced optical bands are used in a hybrid FSO-OF system to increase transmission range, reduce signal loss, and improve the stability of modern optical networks. However, a RoF system ensures transmission stability over long distances. Hybrid RF/FSO systems naturally switch between these two technologies based on the environment. Thus, they are ideal for 5G, smart cities, and secure communications [12,13].

2.3.2. Factors affecting optical transmission

Several critical factors affect transmission in optical communication systems. Attenuation represents the loss of signal power as it propagates through OF or FSO, measured in decibels per kilometer (dB/km). As a note, the 1550 nm wavelength has the lowest attenuation, making it the optimal choice for long-distance transmissions. Additionally, dispersion distorts signals because different parts of the light travel at varying speeds. It primarily manifests itself in three ways: Multimode Dispersion (MD) in OF technology, which occurs because the light takes different paths and causes the pulses to spread out and overlap; Chromatic Dispersion (CD), which occurs as a result of variations in refractive index as a function of wavelength, causing light to travel at different speeds; and Polarization Mode Dispersion (PMD), which occurs because OF technology is birefringent, causing the polarization states to travel at different speeds. Finally, interference also disrupts transmission; this includes ElectroMagnetic Interference (EMI), where RF signals are affected by other electronic devices or radio sources. Additionally, solar scintillation in deep space communications can occur due to fluctuations in solar wind plasma, and pointing errors can result in the loss of communication if FSO links become misaligned [13,14].

2.3.3. Comparison between FSO and RoF channels

FSO and RoF are two distinct transmission technologies. FSO transmits data wirelessly through air or vacuum using lasers, offering high throughput (several Gbps), very low latency, and good security thanks to its narrow beam. It is inexpensive to deploy since it does not

require cables. However, its range is limited (a few kilometers), and its performance is severely degraded by atmospheric conditions such as fog, rain, turbulence, and physical obstructions. On the other hand, RoF uses wired OF, which has a very high throughput (several Tbps), is entirely immune to adverse weather conditions, is highly reliable due to minimal interference, and can cover long distances (hundreds of kilometers). Its latency is low, but it's slightly higher than FSO's due to the propagation delay in the OF. The main problem with it is that setting up the OF is expensive, and its security is only moderate because it can be hacked by plugging it in. FSO is better for satellite links, urban communications, and 5G backhaul, while RoF is better for 5G networks, remote radio head connections, and broadband internet [15-17].

2.4 Optical multiplexing and demultiplexing

Coherent optical communication systems using Wavelength Division Multiplexing (WDM) (see Figure 2.4) have almost exhausted all the degrees of freedom available in Single-Mode Fibers (SMF) (time, frequency, polarization, and phase). Their capacity is now growing logarithmically, insufficient in the face of the exponential growth of global traffic.

To cost-effectively increase capacity, SDM (Spatial Division Multiplexing) is proposed as a fundamentally new approach. It allows autonomous data streams to be transmitted in parallel over additional spatial channels, such as:

- Multi-core Multiplexing (MCF): A single fiber contains multiple independent cores.
- Mode Division Multiplexing (MDM): A single large-core fiber carries multiple spatial modes (using FMF: Few-Mode Fibers or MMF: Multi-Mode Fibers).

In short, WDM has been very important for getting the most out of single-mode fibers, but it is now at its physical limits. SDM is important for the future because it makes new transmission channels through space (cores or modes). This is the only realistic way to keep up with the growing demand for data rates (see Figure 2.5) [18].

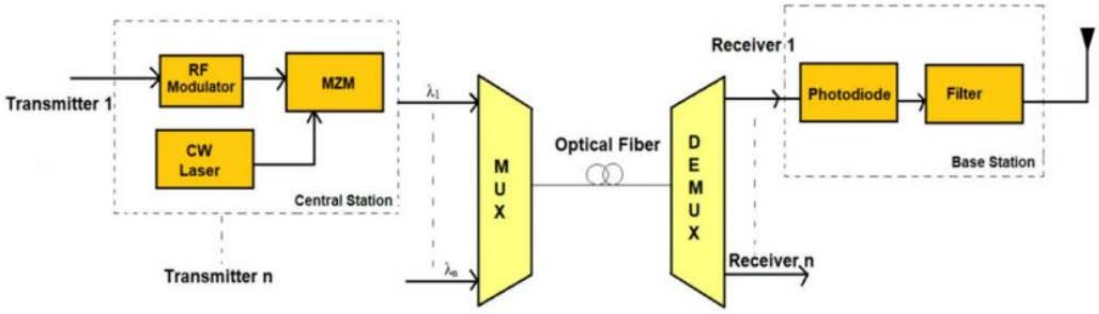

Figure 2.4. Architecture of WDM-based RoF system [19].

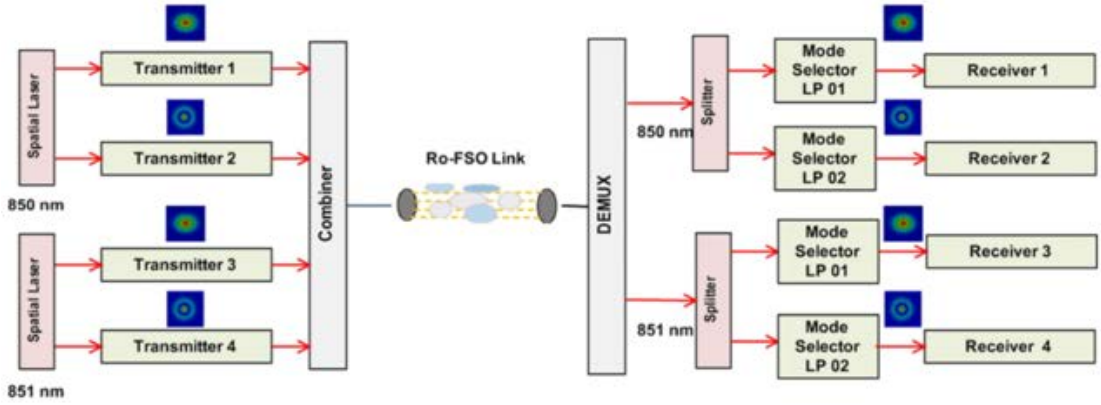

Figure 2.5. Architecture of WDM-SDM-based RoFSO system [20].

2.5. Optoelectronic receivers

2.5.1. Reception modules for RoFSO and RoF

The receiving module of RoF or RoFSO systems is made to demodulate and restore signals that have been sent quickly and effectively, while also making them more stable and reducing interference [21].

2.5.2. Photo-detectors

The photodiode features a PNJ with a P-type semiconductor region on the side that receives light and an N-type semiconductor region on the side that serves as the substrate, see Figure 2.6. A depletion layer forms between the P-layer and N-layer when a reverse bias is applied to the PNJ. This is because the depletion layer has no mobile carriers. When light with more energy than the semiconductor band gap energy hits the area around the intersection of the photodiode (the depletion layer and the surrounding area), the electrons in the valence band absorb the light and move up to the conduction band. This makes holes in the valence band and creates carriers. The carriers thus generated in the depletion layer separate due to the electrical field's conductivity so that the electrons move to the N region, and the holes move to the P region. At this time, the number of carriers generated is essentially proportional to the luminance of the light, and a photocurrent flows through the photodiode. The size of the photocurrent is roughly proportional to the intensity of the light [22,23].

There are three layers in a PIN photodiode: a P-type layer, an intrinsic (I) layer, and an N-type layer, see Figure 2.7. However, the undoped intrinsic layer is essential for enhancing the photodiode's performance. As a result, as light strikes the photodiode, photons of acceptable

energy excite the electrons in the intrinsic layer, producing electron-hole pairs. The electric field already present in the depletion region pushes the electrons toward the P-type region. The movement of charge carriers generates a photocurrent that is directly proportional to the intensity of the light striking it. The intrinsic layer increases the depletion region, reducing the photojunction capacitance of the PIN photodiode. The intrinsic layer absorbs more light, enabling the device to perform faster and more efficiently. Due to this, PIN photodiodes are best conformed for systems that need rapid data transmission employing light and for applications that necessitate the detection of low light levels [25].

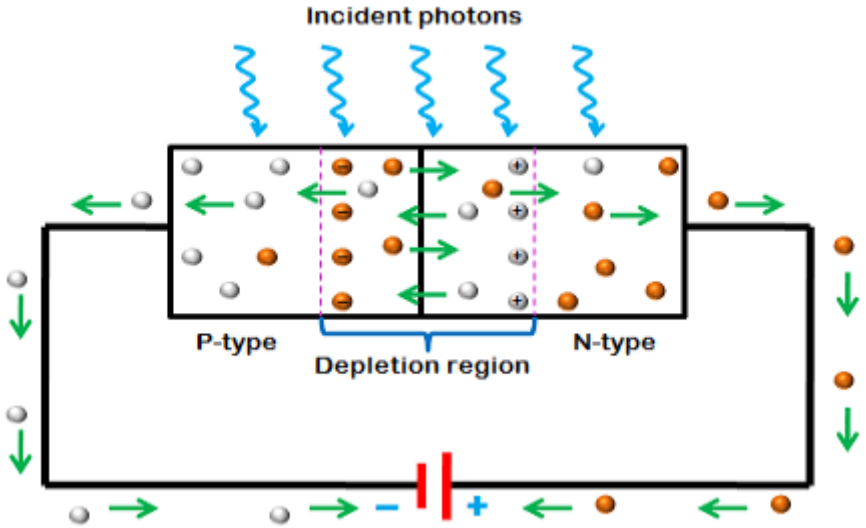

Figure 2.6. PN photo-diode [24].

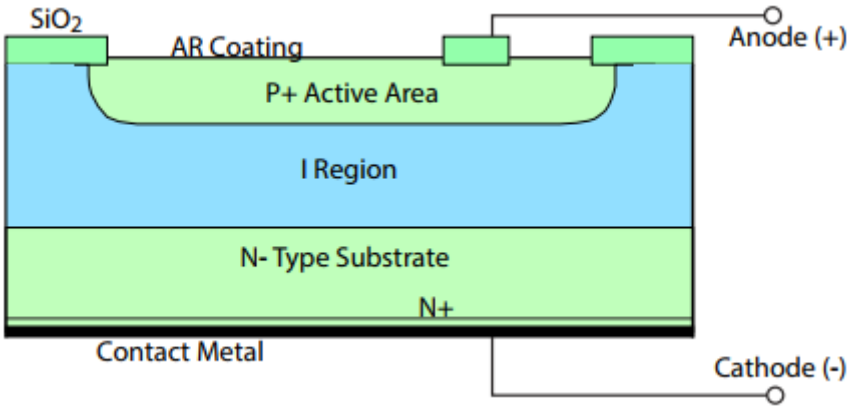

Figure 2.7. PIN Photodiode [26].

An Avalanche Photo-Diode (APD) operates with a high reverse bias, allowing it to amplify internal signals, as shown in Figure 2.8. When a photon strikes the depletion region, it produces electron-hole pairs, which gain energy and undergo impact ionization, thereby expanding the number of charge carriers. This makes the electrical signal stronger, which

makes APD very sensitive to weak light. They work great for taking pictures in low light, for fiber-optic communication, etc [26].

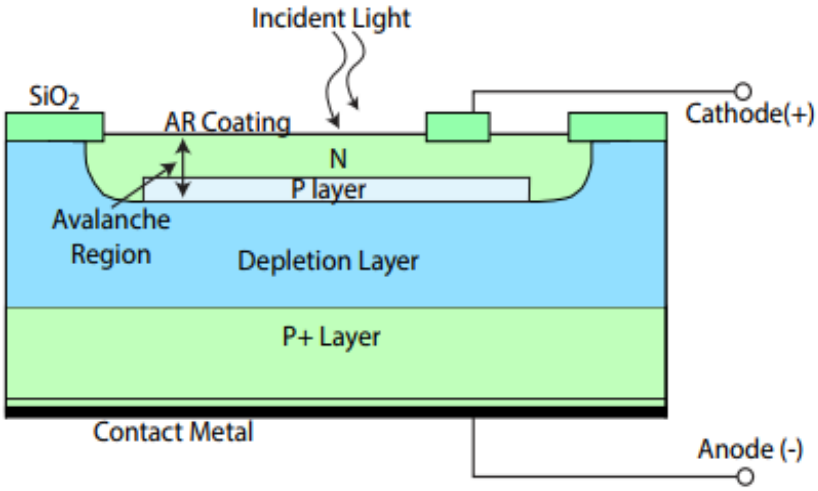

Figure 2.8. Avalanche photodiode [26].

2.5.3. Optical-to-RF and RF-to-optical conversions

RoF is a bidirectional conversion technology that lets OFs send and receive both RF and optical signals. In RoF, a transmitter modulates the RF signal of a light source, such as a laser. This makes an optical signal that sends the information through the OF. At the other end, a demodulator turns the optical signal into an RF signal. However, the opposite is true when it comes to changing optical signals into RF signals. This technology has a lot of benefits, such as being able to send signals over very long distances with little loss, being small, and being very resistant to electromagnetic interference. Also, RoFSO technology is all about converting optical signals to RF signals and vice versa. This technology takes the idea of RoF and applies it to wireless transmission through light in the air [27,28].

2.6. Compensation and correction of errors

Optical amplifiers like Fiber Raman Amplifiers (FRAs), Erbium-Doped Fiber Amplifiers (EDFAs), and Semiconductor Optical Amplifiers (SOAs) are employed to make up for the loss of optical signals over OFs or FSO links. Further, phase shifters are also used to correct phase deviations and reduce phase noise in the system. Furthermore, the self-mixing zero-difference detection technology is also crucial for decoding high-frequency signals, minimizing distortions, and improving signal recovery [21,29-32].

2.7. Improve reliability and performance

The use of differential reception technology proves to be safe for extracting baseband signals, as it effectively eliminates high-frequency interference. In addition, the eye diagram indicates that the system maintains a stable and clear signal even after transmitting FSO waves over a distance of 1 km, demonstrating its robustness. RF spectrum analysis confirms the stability of MMW generation at 60 GHz and the accuracy of signal decoding. Together, these elements improve system performance, ensuring fast and reliable data transmission over a hybrid RoF-RoFSO link [21].

2.8. Receiver performance criteria

The electronic circuits that convert incoming optical signals into electrical signals, must satisfy distinct basic performance measures to detect and process signals with accurately. Sensitivity, in [dBm], is the minimum optical power needed to perform a specified Bit Error Rate (BER). Responsivity (R) in [A/W] is the amount of electrical current that is produced for each unit of optical power that is received. Performance in noise, influenced by thermal noise, particle noise, and current in the dark, directly affects the Signal-to-Noise Ratio (SNR). Dynamic range defines the effective spectrum of optical input power that a device can accurately process. BER is a crucial measure that signifies the likelihood of errors per bit, where a reduced value denotes superior performance. Linearity guarantees a proportional correlation between input power and output signal. Power consumption is essential to overall system efficiency. Ultimately, spectral sensitivity delineates the spectrum of operational wavelengths (e.g., 850 nm, 1310 nm, 1550 nm) for which the receiver is engineered [33-35].

2.9. Conclusion

This chapter covers the various optoelectronic elements that comprise the RoF and RoFSO communication link. We also discuss the performance of optoelectronic receivers, multiplexing strategies as WDM and SDM, amplification techniques as EDFA, SOA an FRA, and advanced transceivers. Furthermore, existing communication networks have a good opportunity to benefit from the development of FSO and RoF technologies. To improve the efficiency and reliability of optical transmission, several issues still need to be addressed. In the next chapter, we summarize the proposed contribution of this project.

2.10. References of chapter 2

1. Kumar, A., & Krishnan, P. (2025). Performance analysis of multi-RIS enabled RoFSO system for V2I communications. Optical and Quantum Electronics, 57(6), 1-26.

2. Sarita, S., Sharma, N., Agrawal, S., & Budhiraja, S. (2025). Analysis and performance improvement of 60 GHz mm-wave based hybrid RoF and RoFSO system under atmospheric turbulence using FFE+ DFE electronic equalizer. Optical and Quantum Electronics, 57(2), 1-41.
3. Al-Gailani, S. A., Salleh, M. F. M., Salem, A. A., Shaddad, R. Q., Sheikh, U. U., Algeelani, N. A., & Almohamad, T. A. (2020). A survey of free space optics (FSO) communication systems, links, and networks. *IEEE Access*, *9*, 7353-7373.
4. Kressel, H., Ettenberg, M., Wittke, J. P., & Ladany, I. (2005). Laser diodes and LEDs for fiber optical communication. *Semiconductor devices for optical communication*, 9-62.
5. Ribbens, W. (2017). *Understanding automotive electronics: an engineering perspective*. Butterworth-heinemann.
6. Sharma, S. K., da Silva, C. J., Garcia, D. J., & Shrivastava, N. (Eds.). (2022). *Modern Luminescence from Fundamental Concepts to Materials and Applications, Volume 1: Concepts of Luminescence* (Vol. 1). Woodhead Publishing.
7. Merzougi, S. M. (2022). Transmission simultanée fixe FTTH et mobile 5G sur fibre optique basée sur les modulations à double polarisation. (PFE ; Université Abou berk Belkaïd- Tlemcen).
8. Dasan, M., Francis, F., Sarath, K. T., Dipin, E., & Srinivas, T. (2019). Optically multiplexed systems: wavelength division multiplexing. In *Multiplexing*. IntechOpen.
9. Hernandez, S., Peucheret, C., Da Ros, F., & Zibar, D. (2024). End-to-end optimization of optical communication systems based on directly modulated lasers. *Journal of Optical Communications and Networking*, *16*(8), D29-D43.
10. Biglieri, E., Proakis, J., & Shamai, S. (2002). Fading channels: Information-theoretic and communications aspects. *IEEE transactions on information theory*, *44*(6), 2619-2692.
11. Boukharouba, A. (2018). Communications Numériques : Transmission en bande de base. https://dspace.univ-guelma.dz.
12. Rahman, M. T., Rahman, M., Hossain, M. M., & Hossain, M. S. (2023). Integration of Optical and Free Space Optics Network Architecture for High-Speed Communication in Adverse Weather using suitable Optical Bands. Optical Bands, 11(2), 291-298.
13. Bopardikar, R., Joseph, C., & Raj, A. B. A Review Paper on Hybrid RF/FSO System for Communication. International Journal of Engineering Research and Reviews, 12(3), 90-115.

14. BOUZID, C., & NOUARI, A. (2022). Etude de l'influence de l'atténuation et la dispersion sur la transmission à fibres optiques. (PFE, Université de Kasdi Merbah-Ouargla).
15. Chaudhary, S., Wuttisittikulkij, L., Nebhen, J., Tang, X., Saadi, M., Al Otaibi, S., ... & Choudhary, S. (2021). Hybrid MDM-PDM based Ro-FSO system for broadband services by incorporating donut modes under diverse weather conditions. Frontiers in Physics, 9, 756232.
16. Malik, A., & Singh, P. (2015). Free space optics: current applications and future challenges. International journal of optics, 2015(1), 945483.
17. Barnoski, M. K., & Personick, S. D. (2005). Measurements in fiber optics. Proceedings of the IEEE, 66(4), 429-441.
18. Weng, Y., Ip, E., Pan, Z., & Wang, T. (2016). Advanced spatial-division multiplexed measurement systems propositions—from telecommunication to sensing applications: a review. *Sensors*, *16*(9), 1387.
19. EBRAHIM, L. L., & ATROSHEY, S. M. S. (2022). Review on radio over fiber systems for capacity enhancement. Journal of Duhok University, 25(2), 482-506.
20. Shakthi Murugan, K. H., Sharma, A., & Malhotra, J. (2020). Performance analysis of 80 Gbps Ro-FSO system by incorporating hybrid WDM-MDM scheme. Optical and Quantum Electronics, 52, 1-12.
21. Tian, Q., Shao, Y., Wang, A., Yang, J., Wang, Z., Yu, N., ... & Zuo, R. (2022). A RoF-FSO communication system using 10Gbit/s polsk 4-PAM downstream signals. In *ITM Web of Conferences* (Vol. 45, p. 02004). EDP Sciences.
22. Donati, S. (2021). *Photodetectors: devices, circuits and applications*. John Wiley & Sons.
23. Culshaw, B. (1986). Photodetectors and photodetection. *Sensors and Actuators*, *10*(3-4), 263-285.
24. https://www.physics-and-radio-electronics.com/electronic-devices-and-circuits/semiconductor-diodes/photodiodesymboltypes.html. Accessed 06/12/2025 at 11:38 a.m.
25. Mane, S. (2024). Theoretical Aspects on Photodiodes System: Mechanism, Modes and Types. *International Journal of Multidisciplinary Innovation and Research Methodology, ISSN: 2960-2068, 3 (1)*, 52-60.
26. https://www.teamwavelength.com/download/applicationtechnotes/an-ld17.pdf?srsltid=AfmBOooGLhp08puMyHXA4z22I8ynp0MiTt6_ooOR5x_cdiHR4XCrpCKd. Accessed 06/12/2025 at 12:12 a.m.

27. Wang, X., Chan, E. H., & Minasian, R. A. (2013). Optical-to-RF phase shift conversion-based microwave photonic phase shifter using a fiber Bragg grating. *Optics Letters*, *39*(1), 142-145.
28. Williamson, R. C., & Esman, R. D. (2008). RF photonics. *Journal of Lightwave Technology*, *26*(9), 1145-1153.
29. Masuda, H. (2006). Recent progress on optical fiber amplifiers and their applications. Active and Passive Optical Components for Communications VI, 6389, 8-17.
30. Zervas, M. N., & van den Hoven, G. (2001). Optical amplifiers. In Fibre Optic Communication Devices (pp. 151-196). Berlin, Heidelberg: Springer Berlin Heidelberg.
31. Fathi, M. T., & Donati, S. (2012). Simultaneous measurement of thickness and refractive index by a single-channel self-mixing interferometer. IET optoelectronics, 6(1), 7-12.
32. Li, W. T., Chiang, Y. C., Tsai, J. H., Yang, H. Y., Cheng, J. H., & Huang, T. W. (2013). 60-GHz 5-bit phase shifter with integrated VGA phase-error compensation. IEEE Transactions on Microwave Theory and Techniques, 61(3), 1224-1235.
33. Vera-Marquina, A., Martínez-Castillo, J., Zaldívar-Huerta, I. E., & Díaz-Sánchez, A. (2014). Performance evaluation of an integrated optoelectronic receiver. Journal of applied research and technology, 12(1), 45-51.
34. Das, T. (2013). Practical considerations for low noise amplifier design. Freescale Semiconductor, 10, 1-10.
35. Breems, L., & Huijsing, J. (2001). Continuous-time sigma-delta modulation for A/D conversion in radio receivers (Vol. 634). Springer Science & Business Media.

CHAPTER 3

Study and evaluation of a 5G MMW transmission system using RoMMF-FSO for a 5GBUN

3.1. Introduction

This chapter presents comprehensive simulation results evaluating the performance of RoMMF-FSO (Radio over MultiMode Fiber-Free Space Optical) communication systems under different Atmospheric Turbulence (AT) conditions. However, the simulations specifically analyze the propagation of various Laguerre-Gauss modes (LG_{00}, LG_{01}, LG_{02}, and LG_{03}) through low (C_n^2 = 1e-17 $m^{-2/3}$), medium (C_n^2 = 1e-15 $m^{-2/3}$), and strong (C_n^2 = 1e-13 $m^{-2/3}$) AT environments while considering different Weather Conditions (WCs) levels (light, medium and heavy). In addition, the study aims to characterize the combined impact of these environmental factors on wireless optical transmission using the SDM technique to increase transmission capacity. Finally, the performances measured to assess the effectiveness of the proposed system are BER (≤1e-9), Q-Factor (≈6), and Communication Capacity (CC) [1-8].

3.2. Proposed 5G network

With the massive data transfers and increasing data rates, modern communication technologies are indispensable for effective communication. This work proposes a 5G communication system dedicated to emergency applications (see Figure 3.1), using the 24 GHz, 26 GHz, 28 GHz, and 30 GHz MilliMeter-Wave (MMW) frequency bands [9,10]. The network deploys connectivity linking four Unmanned Aerial Vehicles (UAVs) to a Base Station (BS) employing a wireless optical (FSO) link as a relay [11,12]. The key contributions of this work include:

- The study of the effects of variations in AT conditions, Weather Conditions (WCs), and the distance of the FSO link on the performance of the proposed system;
- The analysis of the impact of varying transmit power (PTx) on the combined RoMMF-FSO link;
- A cost analysis based on AT conditions and the 5GBUN (5G Back-Up Network) deployment strategy;
- A comparative study of RoMMF-FSO performance under different atmospheric conditions (weak, medium and strong).

3.3. Proposed system

Figures 3.2 and 3.3 present the configuration diagrams of the proposed models using Optisystem software [13]. They show that the RoMMF-FSO link transmits four 5G MMW signals with four different LG-type modes, with the following distribution: LG_{00}→ 24 GHz,

LG_{01}→ 26 GHz, LG_{02}→ 28 GHz, and LG_{03}→ 30 GHz, each with an amplitude of 1, a polarization of 0, and a phase of 90 degrees, at a data rate of 10 Gbps (see Figures 3.4 and 3.5). The use of SDM technology enables the proposed system to achieve a remarkable total data rate of 40 Gbps at a wavelength of 850 nm [6-8,14-16].

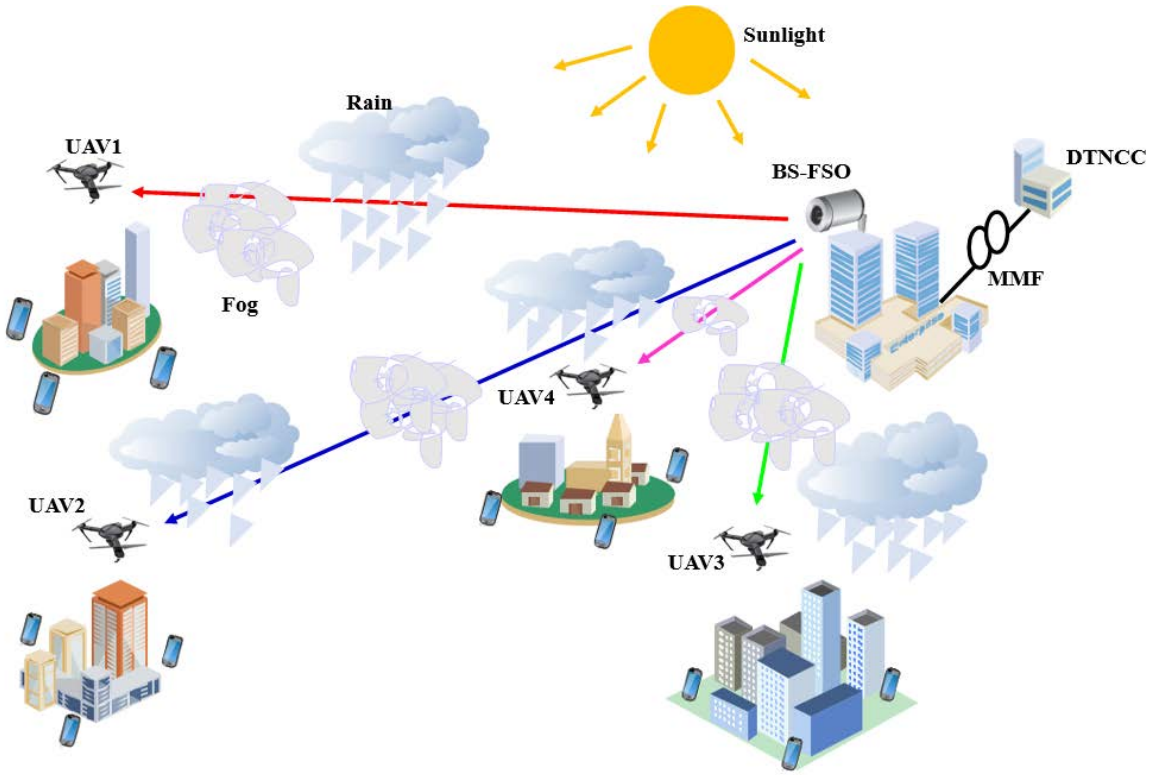

Figure 3.1. Proposed network using 5G MMW over RoMMF-FSO.

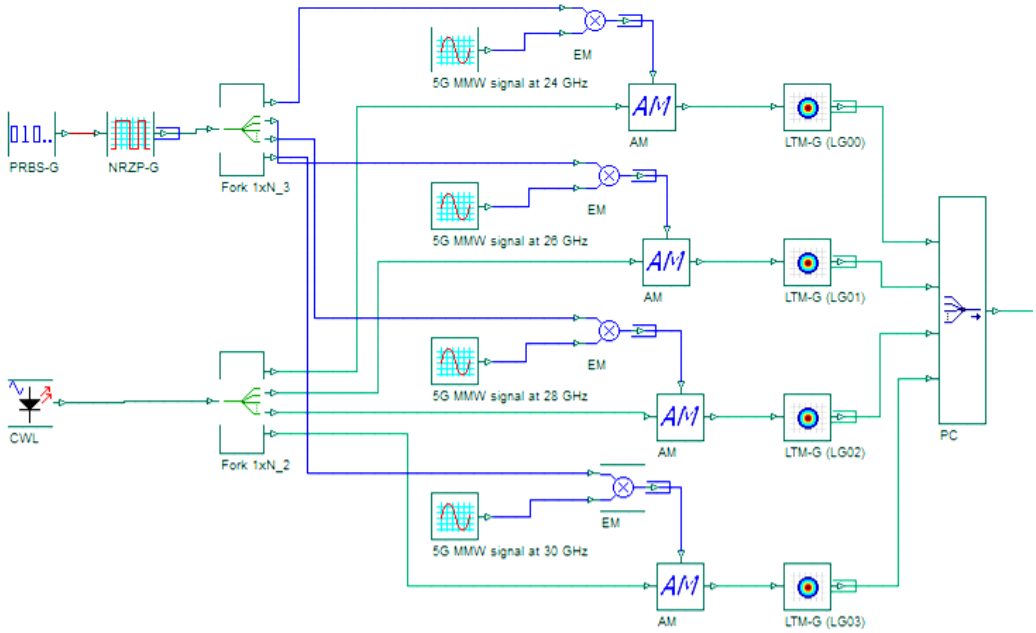

Figure 3.2. Transmitter of the four 5G MMW signals using SDM technology.

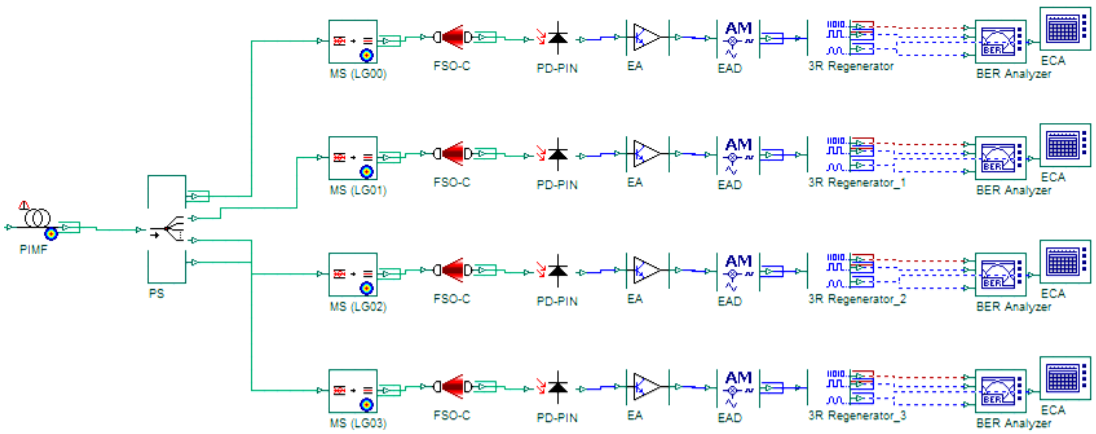

Figure 3.3. RoMMF-FSO link and receiver part of each 5G MMW signal.

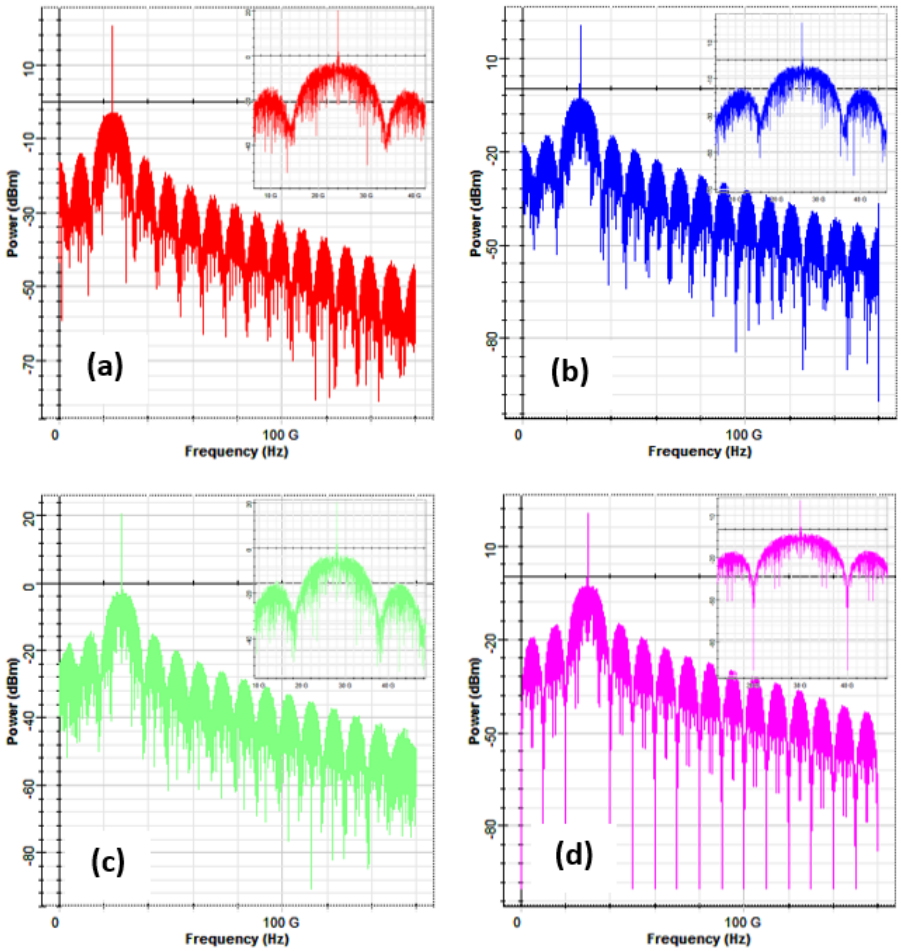

Figure 3.4. 5G MMW electrical signal spectrum: (a) 24 GHz, (b) 26 GHz, (c) 28 GHz and (d) 30 GHz.

In the proposed configuration for the 5G MMW transmitter, shown in Figure 3.2, 10 Gbit/s binary data is generated ideally using a Pseudo-Random Binary Sequence Generator (PRBS-G). However, this binary data is then transmitted transparently to the Non-Return-to-Zero

Pulse Generator (NRZP-G), located in the same part of the 5G MMW transmitter, for encoding. Therefore, the transmitted NRZP-G downlink data is expressed through the following formula:

$$z(t) = \sum d_k \cdot g_T(t - k \cdot T_s) \quad (1)$$

Where d_k symbolizes the binary data, $g_T(t)$ stands for the code's waveform function, which is a rectangle shape, and T_s stands for the symbol duration [16-18].

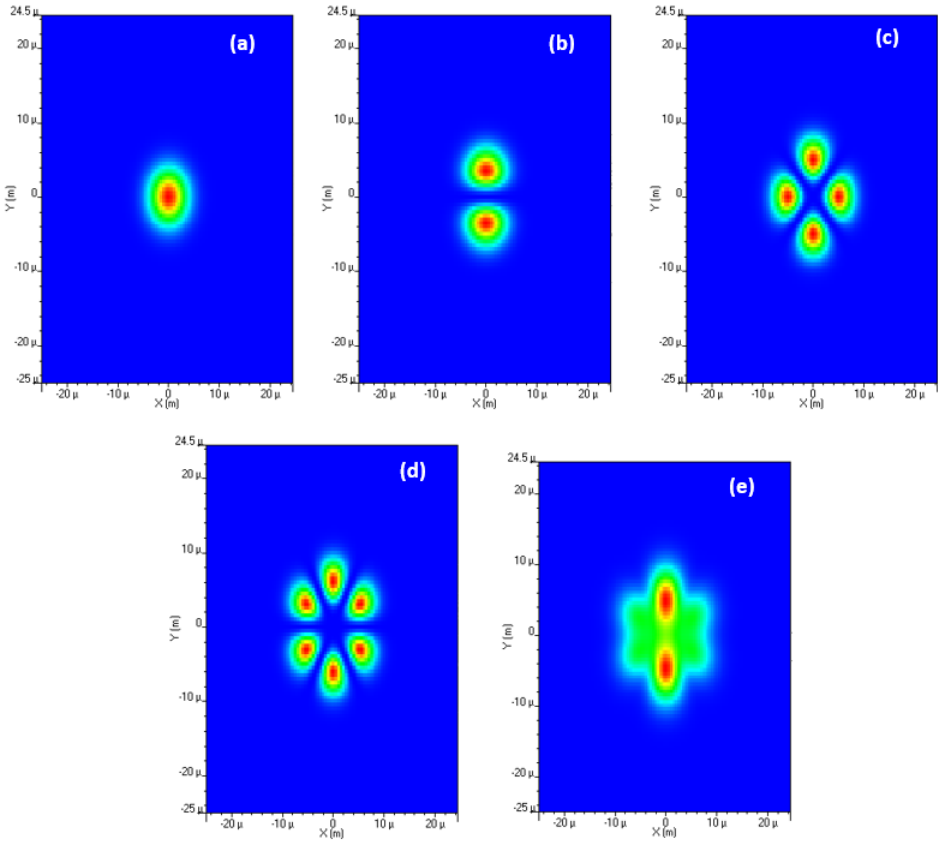

Figure 3.5. Spatial profile of each 5G MMW signal and its total spatial profile: (a) LG_{00}, (b) LG_{01}, (c) LG_{02}, (d) LG_{03} and (e) total spatial profile.

Figure 3.2 illustrates the complex interaction of the emission part components in the proposed system. First, the Continuous Wave Laser (CWL) produces an optical signal (see equation (2)) for each part of the 5G MMW signals using the main parameters: wavelength of 850 nm, power of 10 dBm and linewidth of 10 MHz. However, the encoded data $z(t)$ takes a central place, modulating by the 5G MMW electrical signal via the electrical multiplier component.

$$Op_s(t) = A_{Op_s} \cdot e^{jwop_s \cdot t} \quad (2)$$

Where, $Op_s(t)$ represents the CWL optical signal to the optical Amplitude Modulator (or AM), A_{Op_s} represents the amplitude, and w_{Op_s} represents the angular frequency of the CWL [16-18].

Furthermore, before the four 5G MMW signals are multiplexed by SDM technology, each 5G MMW signal must pass through an external AM optical modulator. This modulator modulates the optical carrier with the electrical modulation signal, i.e., the 5G MMW signal. Let $Op_s(t)$ denote the input optical signal to the optical AM; therefore, the resulting equation describes the exact output behavior of the AM, expressed by:

$$OOp_S(t) = Op_s(t) \cdot \sqrt{Mod_{AM}(t)} \quad (3)$$

However, the AM output optical signal, $OOp_S(t)$, depends on the following modulation function, $Mod_{AM}(t)$,

$$Mod(t) = (1 - MI) + MI \cdot EI_S(t) \quad (4)$$

Where, MI is the modulation index and $E_{I_s}(t)$ is the 5G MMW input electrical signal. Thus, the electrical sinusoidal component of the 5G MMW signal (which is the Local Oscillator (or LO) in the 5G MMW transmitter of the DTNCC: Data Transmission and Network Control Center) can generate $E_{I_s}(t)$ at different frequencies, such as: 24 GHz, 26 GHz, 28 GHz, and 30 GHz.

$$E_{I_s}(t) = z(t) \cdot [E_{I_{MMW}} \cdot \cos(w_{MMW} \cdot t)] \quad (5)$$

Where, $E_{I_{MMW}}$ represents the amplitude of the 5G MMW signal and w_{MMW} represents the angular frequency of the 5G MMW signal [16-18].

All 5G MMW signals are modulated using optical AM and then transmitted employing the LTM-G (Laguerre Transverse Mode Generator) component, which is designed to transform single-mode signals into multimode signals. The purpose of this operation is to couple the X and Y polarizations of the input signal ($OOp_S(t)$) with Laguerre-Gaussian (LG) profiles, such as: LG_{00}, LG_{01}, LG_{02}, and LG_{03}. This coupling is essential because it allows the power distribution required for converting single-mode signals into multimode signals (see Figure 5). The LG mode is a method for describing a laser beam by its transverse intensity and phase profile. However, the LG mode can be described mathematically as follows [19,20]:

$$\psi_{n,m}(r,\phi) = \left(\frac{2\cdot r^2}{{w_0}^2}\right)^{\left|\frac{n}{2}\right|} L_m^n\left(\frac{2\cdot r^2}{{w_0}^2}\right) e^{\left(\frac{r^2}{{w_0}^2}\right)} e^{\left(j\frac{\pi\cdot r^2}{\lambda R_0}\right)} \begin{cases} \sin(|n|\phi), & n \geq 0 \\ \cos(|n|\phi), & n < 0 \end{cases} \quad (6)$$

Where, $\psi_{nm}(r,\phi)$ is the spatial intensity distribution, r, and ϕ represent the radial coordinates, n, and m are the X and Y index that define the azimuthal and radial indexes, respectively. R_0 is the radius of curvature, and w_0 is the beam size. L_m^n is the Laguerre polynomial. When the Complex parameter is enabled, a complex mode output with sin and cos terms is generated, otherwise the output is real and it depends on the signal of the n parameter [19,20].

The present analysis performs a transmission rate of 40 Gbps for one lambda (i.e., 850 nm) by transmitting four 5G MMW signals over beams of varying dimensions. To generate the LG modes, the system uses different experimental methodologies (see Figure 3.5). Finally, to combine the LG modes of the 5G MMW signals into a single beam and transmit them over the RoMMF-FSO link, the Power Combiner (PC) is used [16].

Before discussing the type of channel distribution used for the four FSO links in each bundle, as shown in Figure 3.3, a kind of MMF component called PIMF (Parabolic Index Multimode Fiber) is used to connect the DTNCC and the FSO BS relay with a distance of 500 m. This component is a MMF with a parabolic refractive index. It is a spatially dependent component that models the transverse field profiles and propagation constants for all modes supported by the fiber [21-23].

The Power Splitter (PS 4x1) component (see Figure 3.3) is essential for maintaining the quality of the Received Optical Power Beam (ROPB) for all 5G MMW signals (see Figure 3.6). It does this by splitting the power into four optical output signals after reception at the end of the PIMF component (P_{ROPB}). The output ROPB of each PS port ($P_{r_{PS}}$) is decreased by:

$$P_{r_{PS}} = \frac{P_{ROPB}\cdot 10^{\frac{-AT_{PS}}{10}}}{2} \quad (7)$$

Where, AT_{PS} represents the power attenuation at the PS, and the loss is imposed on the ROPB during division.

After using the PS component, the MS (Mode Selector) component appeared. The MS allows extracting a single mode from a multimode signal. In this case, we focus on the specific mode

of each 5G MMW signal, which corresponds for example to LG_{00}→ 24 GHz, LG_{01}→ 26 GHz, LG_{02}→ 28 GHz, and LG_{03}→ 30 GHz (see Figure 3.3).

Regarding the channel model used for the FSO link, it is of the Gamma-Gamma (GG) type, as it is the most realistic. GG Distribution (GGD) is not only a tool for simulating the FSO channel, but it also plays a crucial role in determining the vortices in the GG fading model. As shown in Figure 3.3, the GGD is used to simulate all FSO channels, which realistically support the transport of the four 5G MMW signals [16-18, 24,25].

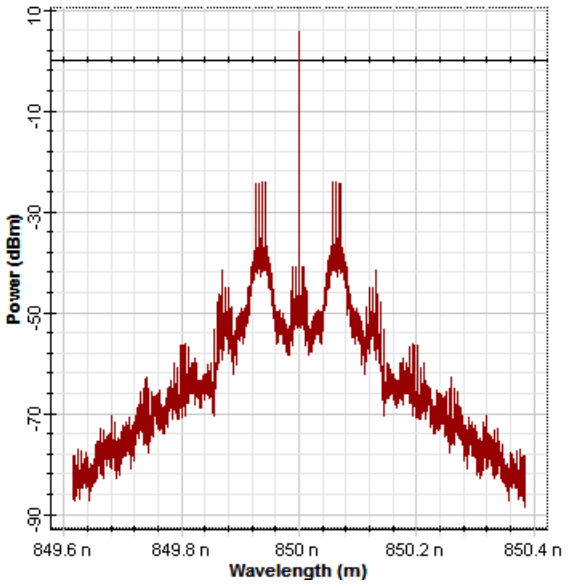

Figure 3.6. ROPB for all 5G MMW signals at the end of PIMF.

Furthermore, the GGD model partitions the normalized light intensity (I) propagating through the FSO channel into small- and large-scale vortices, which are themselves characterized by the GGD of the GG fading model. This results in the following mathematical expression for the PDF [16-18, 24,25]

$$P_{\Gamma\Gamma}(I) = \frac{2(Alpha\cdot Beta)^{\left(\frac{Alpha+Beta}{2}\right)}}{\Gamma(Alpha)\cdot\Gamma(Beta)} \cdot I^{\left(\frac{Alpha+Beta}{2}-1\right)} \cdot K_{Alpha-Beta}(2(Alpha\cdot Beta\cdot I)^{0.5}), I > 0 \quad (8)$$

$$Alpha = \left[exp\left(\frac{0.49\cdot\sigma_R^2}{\left(1+1.11\cdot\sigma_R^{12/5}\right)^{7/6}}\right) - 1\right]^{-1} \quad (9)$$

$$Beta = \left[exp\left(\frac{0.51 \cdot \sigma_R^2}{\left(1+0.69 \cdot \sigma_R^{12/5}\right)^{5/6}} \right) - 1 \right]^{-1}$$

(10)

$$SI = Alpha^{-1} + Beta^{-1} + (Alpha \cdot Beta)^{-1}$$

(11)

$$\sigma_R^2 = 1.23 \cdot C_n^2 \cdot \left(\frac{2\pi}{\lambda_{CWL}}\right)^{7/6} \cdot L^{11/6}$$

(12)

Where the parameters Alpha and Beta are respectively related to the appropriate numbers of small- and large-scale vortices, according to the following equations (9) and (10). $\Gamma(\cdot)$ and $K_{Alpha-Beta}(\cdot)$ represent the Gamma function and second-order Bessel function (Alpha-Beta), respectively. The resulting light intensity (*I*) instabilities, coordinating with the parameters Alpha and Beta, produce the Scintillation Index (SI) as in Eq. (11). This SI is an essential criterion in evaluating the optical receiver's performance, making it necessary to understand the impact of Alpha and Beta, they are suitable for the plane wave beam at the optical receiver.

Furthermore, σ_R^2 denotes the Rytov variance, which is determined employing Eq. (12), $\frac{2\pi}{\lambda_{CWL}}$ is the wavenumber in m, and L is the distance of FSO link in m. Finally, C_n^2 in [m-2/3] corresponds to the refractive index structure parameter of the environment variations, expressed in terms of the AT strength. The values of C_n^2 can vary: 1e-17 $m^{-2/3}$, 1e-15 $m^{-2/3}$, and 1e-13 $m^{-2/3}$ indicate weak, moderate, and strong AT, respectively. The crucial factor that describes the impact of the AT on the optical beams propagating through the FSO channel is C_n^2 [16-18, 24-26].

On the other hand, for losses related to the FSO environment, adverse WCs cause an exponential attenuation h_L of the information transmitted by the laser beam between the transmitting telescope and the receiving telescope of the FSO channel. The Beer-Lambert law formula (13) can explain this phenomenon [16-18,26]

$$h_L = exp(-\sigma L)$$

(13)

Where σ is the Atmospheric Attenuation (or AA) coefficient in dB/km, as derived from:

$$\sigma = \left(\frac{3.91}{V}\right) \cdot \left(\frac{\lambda_{CWL}}{550\ nm}\right)^{-q}$$

(14)

Where, V stands the visibility in km, λ_{CWL} stands the used CWL wavelength in nm, and q is the size of the distribution of scattered particles, defined by the Kim-Kruse model. This research has made it possible to obtain precise values of q for different visibility ranges [16-18,26]

$$q = \begin{cases} 1.6\ (V > 50\ km) \\ 1.3\ (6\ km \leq\ V \leq 50\ km) \\ 0.585 \cdot V^{\left(\frac{1}{3}\right)} (V < 6\ km) \end{cases}$$

(15)

However, it is possible to use the simplest mathematical formula to establish the optical power of the received beam ($P_{r_{FSO}}$) at the receiver of the FSO channel telescope to apply it to each SDM signal (LG_{00}→ 24 GHz, LG_{01}→ 26 GHz, LG_{02}→ 28 GHz, and LG_{03}→ 30 GHz), namely

$$P_{r_{FSO}} = P_{t_{FSO}} \cdot \frac{{D_{r_{FSO}}}^2}{\left(D_{t_{FSO}} + \theta_{FSO} \cdot L_{FSO}\right)^2} \cdot 10^{-\frac{\sigma \cdot L_{FSO}}{10}}$$

(16)

Let's go over the specifics of the FSO channel. $P_{t_{FSO}}$ is the optical power of the beam sent by the telescope transmitter, $D_{r_{FSO}}$ is the diameter of the receiver aperture in m, and $D_{t_{FSO}}$ is the diameter of the transmitter aperture in m. We also have L_{FSO}, which is the distance between the FSO links in meters, and θ_{FSO}, which is the beam divergence in mrad [16-18,26].

Once the $P_{r_{PIN}}$ is received at the PD-PIN, the latter, exploiting the photoelectric effect in its semiconductor junction, transforms an optical signal (such as the specific beams LG_{00}→ 24 GHz, LG_{01}→ 26 GHz, LG_{02}→ 28 GHz, and LG_{03}→ 30 GHz) into a 5G MMW electrical signal. This is then amplified by an Electrical Amplifier (EA), which necessarily introduces thermal noise. A coherent Electrical Amplitude Demodulator (EAD) then recovers the baseband signal envelope from the amplitude-modulated 5G MMW electrical signal, employing a synchronized carrier wave and filtering. The resulting baseband signal can be examined by a 3R regenerator (3R-R), which performs re-amplification, reshaping, and time-reshaping operations, taking into account signals from receivers or after additional demodulations. Finally, a BER analyzer is used to evaluate the reliability and performance of

the proposed system by measuring the BER, which is correlated with the SNR and the link quality (Q-Factor). An Electrical Carrier Analyzer (ECA) measures the SNR.

3.4. Evaluation of the proposed system

To effectively evaluate the performance of the proposed system, it is necessary to be familiar with the channel interference and various noise sources present in the transceivers.

Initially, the $BER_{optical}$ of the optical signal transmitted along the RoMMF-FSO link can be written as follows [16,26-30].

$$BER_{optical} = \int_0^{\infty} BER_{AWGN}(I) \cdot P_{\Gamma\Gamma}(I)\, dI \quad (17)$$

Where,

$$BER_{AWGN}(I) = \frac{1}{2} \cdot erfc\left(\frac{\sqrt{I^2 \cdot \overline{ESNR}}}{2}\right) \quad (18)$$

In this regard, the average Electrical SNR is symbolized by $\overline{ESNR}$, and $erfc$ is the error complementary function.

It is essential to know that, according to Eq. (17), atmospheric optical turbulence, as defined by the GG statistical model, has an impact on the $ESNR$ term.

Basically, $ESNR$ is the ratio of the responsivity R to the scaling of the received optical signal power at PD-PIN ($P_{r_{PIN}}$) and the total noise terms (σ_N^2), which are the thermal noise (σ_{tn}^2), shot noise (σ_{sn}^2) and dark noise (σ_{dn}^2) powers

$$ESNR = \frac{\left(P_{r_{PIN}} \cdot R\right)^2}{\sigma_{tn}^2 + \sigma_{sn}^2 + \sigma_{dn}^2} \quad (19)$$

$$\sigma_{tn}^2 = \frac{4 \cdot k_B \cdot T \cdot B_E}{R_L} \quad (20)$$

$$\sigma_{sn}^2 = 2 \cdot q_e \cdot B_E \cdot P_{r_{PIN}} \cdot R \quad (21)$$

$$\sigma_{dn}^2 = 2 \cdot q_e \cdot B_E \cdot I_d \quad (22)$$

Where, k_B, T, B_E, R_L, q_e, and I_d as Boltzmann's constant, absolute temperature of PD-PIN, electrical bandwidth, load resistance of PD-PIN, electronic load of PD-PIN, and dark current, respectively [16,26-30].

However, the main aspect is that the turbulence and dispersion of air in the studied system have a negative influence on the $ESNR$. This decreases the Communication Capacity (CC) [16]

$$CC = B_E \cdot log_2(1 + \overline{ESNR})$$

(24)

Table 3.1 lists all the parameters used for the proposed system in this work.

3.5. Results and discussion

This section presents the obtained results for the system proposed in this work. The effects of AT (weak (1e-17 $m^{-2/3}$), moderate (1e-15 $m^{-2/3}$), and strong (1e-13 $m^{-2/3}$)) on the RoMMF-FSO link have been examined and analyzed in terms of BER, Q-Factor, and CC based on different WCs (LH: Light-Haze, LR: Light-Rain, LF: Light-Fog, MH: Medium-Haze, MR: Medium-Rain, MF: Medium-Fog, HH: Heavy-Haze, HR: Heavy-Rain, and HF: Heavy-Fog) and varying distances from the FSO link, with the distance from the MMF fixed at 500 m, between the DTNCC and the FSO BS [31,32].

The objective of this contribution is to plan a 5GBUN that connects four mobile BSs with four different frequencies, such as: 24 GHz, 26 GHz, 28 GHz and 30 GHz. For this, we utilize drones (UAVs), which is the most realistic scenario for the type of network proposed in this work, as shown in Figure 3.1.

3.5.1. Effects of AT, WC and the distance of FSO link variations on the performance of the proposed system

The graphical (Figures 3.7, 3.8 and 3.9) representation illustrates the performance parameters (BER, Q-Factor and CC) of the proposed system versus the FSO link distance under varying AT conditions (weak, moderate and strong). The obtained results are organized in a 3x3 matrix for each measurement, showing the performance under light, medium and heavy WC levels with different types, such as: haze, rain and fog.

Operating parameters	Values
Data	Bit rate:10 Gbps, Sequence length: 512[bits, Samples per bit: 32, and Number of samples: 16384.

CW Laser	Wavelength:1552.52 nm, Power: 30 dBm, Linewidth:10 MHz, and Initial phase: 0 deg.
PIMF	Length: 500 m, Attenuation: 2.61 dB/km, dispersion: -100 ps/nm/km
FSO Channel	FSO range is variable, Attenuation coefficient is variable: LH 1.537 dB/km, LR 6.27 dB/km, LF 9 dB/km, MH 4.285 dB/km, MR 9.64 dB/km, MF 16 dB/km, HH 10.115 dB/km, HR 19.28[dB/km, and HF 22 dB/km, Geometrical loss: Yes, Transmitter aperture diameter: 1.5 cm, Beam divergence: 0.1 mrad, Receiver aperture diameter :25 cm, Intensity scintillation: Yes, Scintillation model: Gamma-Gamma, Index refraction structure: variable.
PD-PIN	Dark current :10 nA, Load resistance: 50 Ω, Temperature: 298 K, Responsivity: 0.9 A/W, Thermal power density: 100e-024 W/Hz, Electron charge: 1.6 x 10^{-19} C, and Planck constant: 6.625 x 10^{-34}.
EA	Gain: 15 dB, and Noise power: -60 dBm.
EAD	Carrier wave of local oscillator (frequencies: 24 GHz, 26 GHz, 28 GHz, and 30 GHz), Phase: 0 deg, and Gain: 1. Low pass filter (Cosine roll-off type): Cutoff frequency: 0.75xBit rate Hz, and roll-off factor: 0.9

Table 3.1. Simulation parameters [31,32, proposed].

The BER (see Figure 3.7) curves under weak turbulence conditions, with the LG_{00} (24 GHz for UAV1) mode (red legend), show significantly better performance, with error rates remaining significantly lower over longer distances. In particular, a clear hierarchy exists among the different modes: LG_{00}, LG_{01}, LG_{02}, and LG_{03}, with higher-order modes exhibiting progressively worse BER as the distance increases. However, the dashed threshold line (1e-09, see black legend) corresponds to the acceptable BER limit value for reliable communication between the four UAVs and the FSO BS. The graphs show that the LG_{00} mode (24 GHz for UAV1) can ensure acceptable error rates over longer distances than higher-order modes, such as LG_{01}, LG_{02}, and LG_{03}, at higher frequencies: 26 GHz for UAV2, 28 GHz for UAV3, and 30 GHz for UAV4, respectively, which are more vulnerable to atmospheric attenuation. In addition, the Q-Factor plots show a gradual decrease as the distance increases, with the fundamental LG_{00} mode (24 GHz for UAV1) maintaining higher quality factors over most of the transmission range compared to the other modes operated, LG_{01}, LG_{02}, and LG_{03}. The Q-Factor (see Figure 3.8) degradation follows a more predictable pattern with less dramatic crossover between modes. The acceptable Q-Factor threshold (approximately 6) is maintained over longer distances, indicating that weak-turbulence conditions enable more reliable long-distance communication between the four UAVs and the

FSO BS. For example, to obtain an acceptable BER (1e-09) and Q-Factor (≈ 6), the following distances are required for each UAV link in the LH case: 3437 m (UAV1), 3306 m (UAV2), 3058 m (UAV3), and 2409 m (UAV4). Furthermore, in the MR case, the following distances for each UAV link are, respectively: 1343 m (UAV1), 1319 m (UAV2), 1283 m (UAV3), and 1049 m (UAV4). Finally, for the HF case, the following distances for each UAV link are, respectively: 780.4 m (UAV1), 762 m (UAV2), 744.4 m (UAV3), and 641.5 m (UAV4).

Communication Capacity (CC) measurements (see Figure 3.9) indicate that the LG_{00} mode (24 GHz for UAV1) consistently exhibits higher capacitance ratios across the entire distance range, with a gradual decrease in CC as the FSO distance link increases. For higher-order modes, LG_{01}, LG_{02}, and LG_{03}, CC values are affordable, with a clear separation between the different modes across the entire transmission range. In addition, the CC curves exhibit fewer fluctuations and more predictable behavior, indicating a more stable propagation environment under weak turbulence conditions. As an example, subject to an acceptable BER (1e-09) and a Q factor (≈6), the estimated CCs required for each data transmission from the FSO BS to the UAVs are, in the LH case: 5.326e+10 bps at 3437 m (UAV1), 5.331e+10 bps at 3306 m (UAV2), 5.369e+10 bps at 3058 m (UAV3) and 5.132e+10 bps at 2409 m (UAV4). Furthermore, in the MR case, the estimated CCs are, respectively, 5.344e+10 bps at 1343 m (UAV1), 5.314e+10 bps at 1319 m (UAV2), 5.171e+10 bps at 1283 m (UAV3), and 4.785e+10 bps at 1049 m (UAV4). Finally, for the HF case, the estimated CCs are, respectively, 5.371e+10 bps at 780.4 m (UAV1), 5.316e+10 bps at 762 m (UAV2), 5.291e+10 bps at 744.4 m (UAV3), and 4.946e+10 bps at 641.5 m (UAV4).

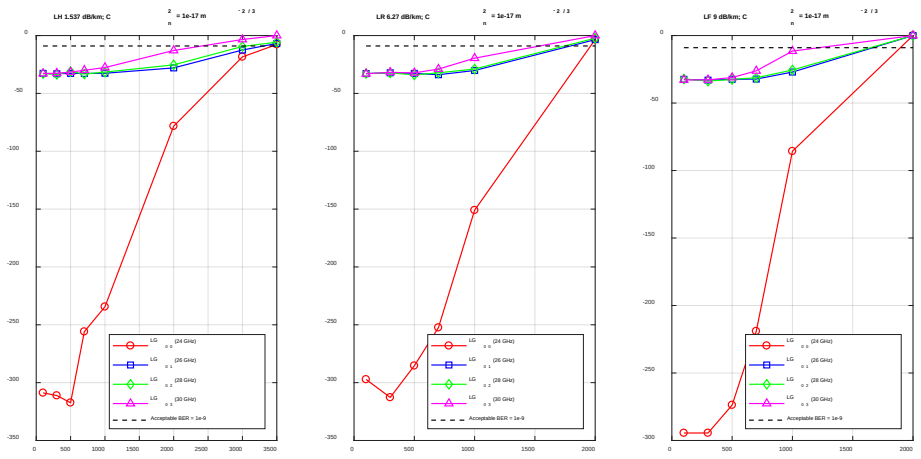

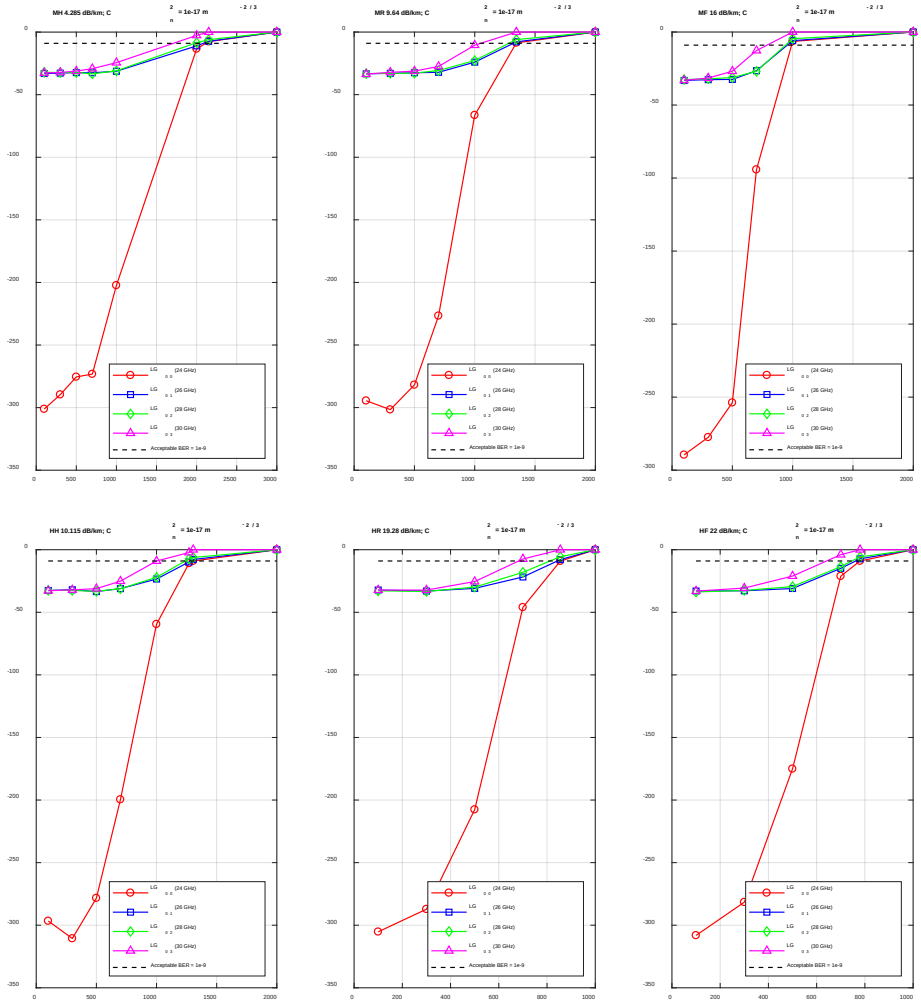

Figure 3.7. Min $\log_{10}$ BER vs. Distance of FSO link [m] under weak AT.

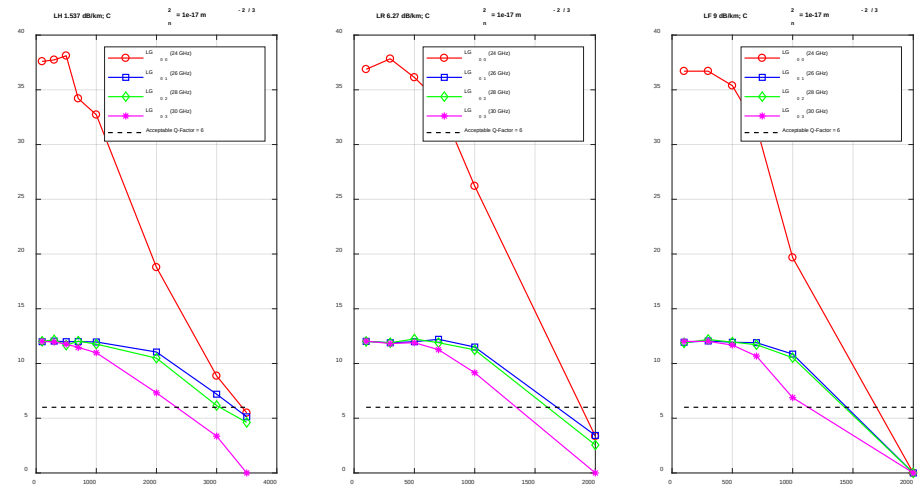

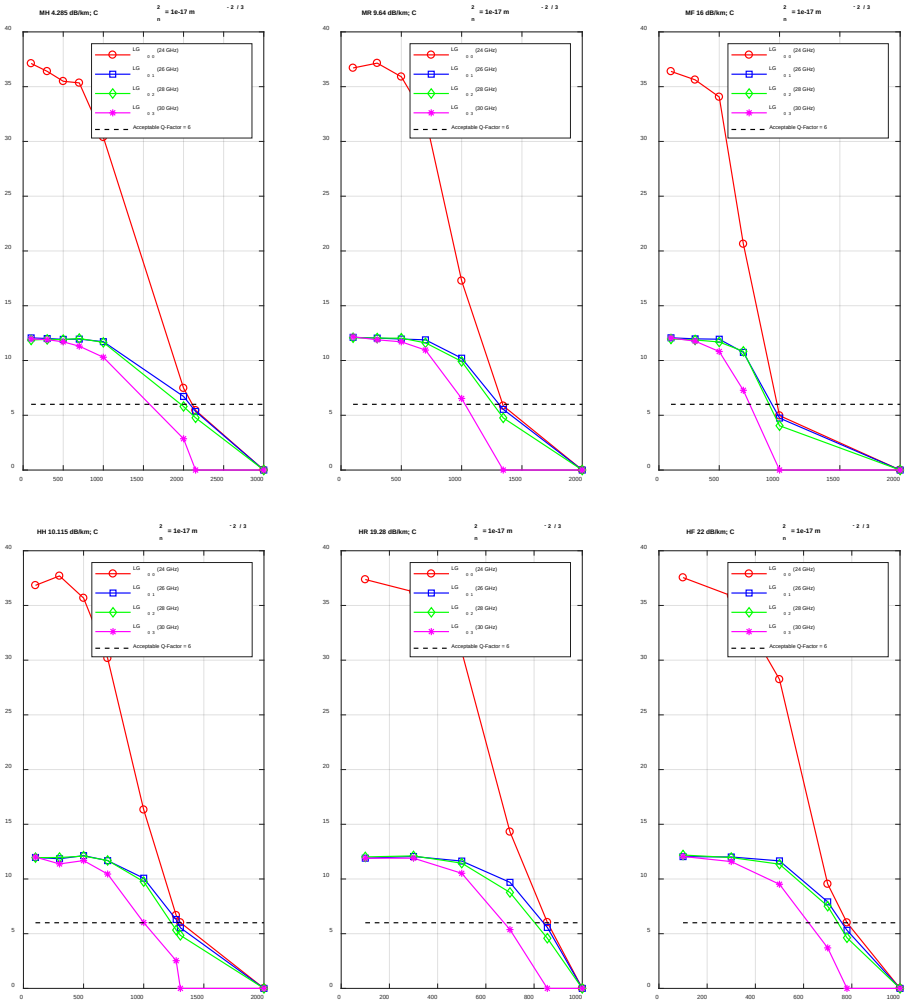

Figure 3.8. Q-Factor vs. Distance of FSO link [m] under weak AT.

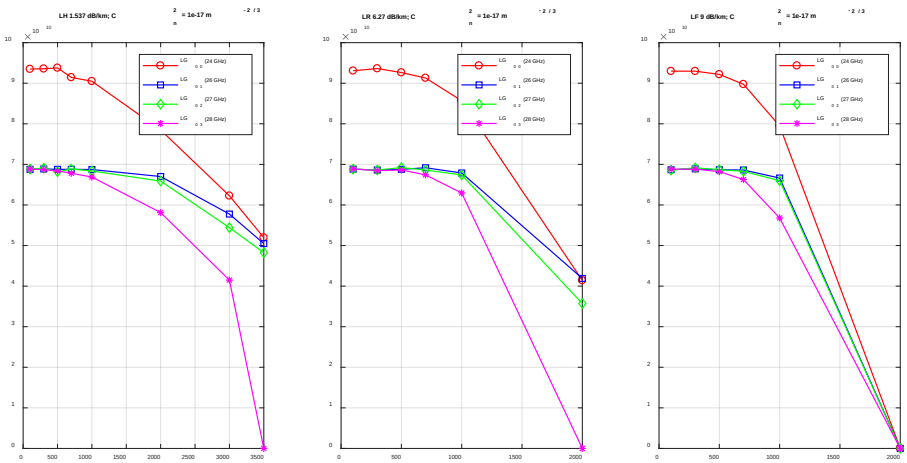

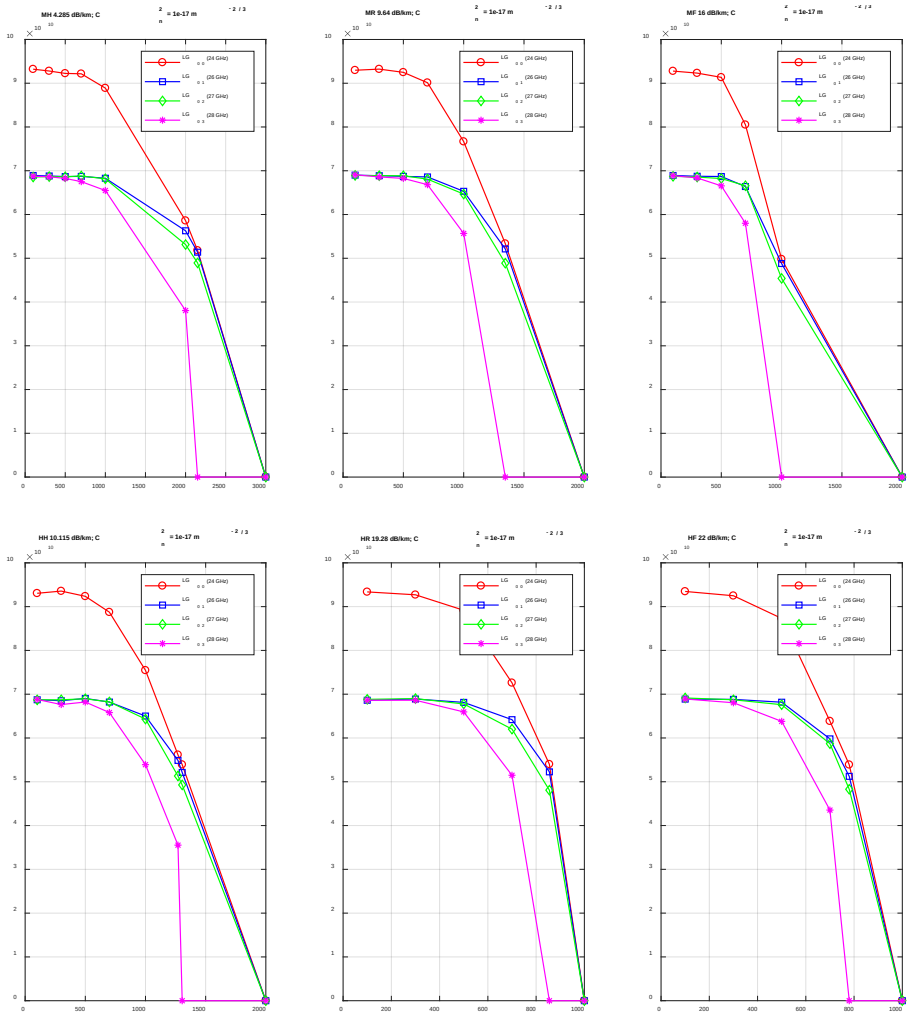

Figure 3.9. CC vs. Distance of FSO link [m] under weak AT.

However, there are significant differences in the BER performance (see Figure 3.10) under moderate turbulence between the following frequencies: 24 GHz (LG_{00} for UAV1), 26 GHz (LG_{01} for UAV2), 28 GHz (LG_{02} for UAV3), and 30 GHz (LG_{03} for UAV4). Remarkably resilient, the 24 GHz frequency (LG_{00} for UAV1) maintains a very low BER over short distances and even long distances before progressively deteriorating as the distance increases. This performance stands out from all other tested frequencies, 26 GHz (LG_{01} for UAV2), 28 GHz (LG_{02} for UAV3), and 30 GHz (LG_{03} for UAV4), which have significantly higher BER values. The difference in performance between 24 GHz (LG_{00} for UAV1) and the other frequencies, 26 GHz (LG_{01} for UAV2), 28 GHz (LG_{02} for UAV3), and 30 GHz (LG_{03} for UAV4), becomes particularly marked under these moderate turbulence conditions, and far exceeds the gap observed in the weak turbulence scenarios. In this context, it is worth noting that only the frequency of 24 GHz (LG_{00} for UAV1) consistently reaches values below the critical BER threshold (approximately 1e-09), which represents the minimum acceptable

performance for reliable communication systems in practical applications, as our 5GBUN aims to achieve.

Furthermore, the Q-Factor measurements (see Figure 3.11) under moderate turbulence conditions confirmed and complemented the results of the BER analysis. For the 24 GHz (LG_{00} for UAV1) frequency, Q-Factor values are exceptional over both short and long distances, establishing a clear performance priority, with this frequency outperforming all other recommendations. The 26 GHz (LG_{01} for UAV2) and 28 GHz (LG_{02} for UAV3) frequencies offer reasonable performance, with Q-Factors typically ranging from [6 to 12]. In contrast, the 30 GHz (LG_{03} for UAV4) frequency has significantly lower values, considering the transmission distance between the FSO BS and the UAVs. This performance stratification becomes more evident as atmospheric conditions deteriorate from light to heavy. The minimum Q-Factor threshold required for reliable communication (approximately 6, as shown in the reference graphs) is consistently met by the 24 GHz (LG_{00} for UAV1) frequency over most short and long distances. This conclusion can also be considered for 26 GHz (LG_{01} for UAV2) and 28 GHz (LG_{02} for UAV3) frequencies, while the 30 GHz (LG_{03} for UAV4) frequency only manages to exceed this threshold over relatively short distances. These results highlight the importance of frequency selection in ensuring acceptable signal quality under moderate turbulence conditions.

For example, to obtain an acceptable BER (1e-09) and Q-Factor (≈ 6), the following distances are required for each UAV link in the LR case: 1651 m (UAV1), 1486 m (UAV2), 1336 m (UAV3), and 600 m (UAV4). Furthermore, in the MH case, the following distances for each UAV link are, respectively: 1763 m (UAV1), 1587 m (UAV2), 1497 m (UAV3), and 610 m (UAV4). Finally, for the HR case, the following distances for each UAV link are, respectively: 892.7 m (UAV1), 809 m (UAV2), 787.3 m (UAV3), and 540 m (UAV4).

The results of the CC analysis (see Figure 3.12) under moderate turbulence conditions reveal a more complex behavior than the other measurements due to the importance of this parameter. In all tested conditions, the 24 GHz (LG_{00} for UAV1) frequency consistently remains the best performer. It is interesting to consider that, the 26 GHz (LG_{01} for UAV2) and 28 GHz (LG_{02} for UAV3) frequencies display competitive performance in almost all scenarios, suggesting potential alternative options for specific deployment conditions of a 5GBUN. The 30 GHz (LG_{03} for UAV4) frequency represented by the pink curve consistently displays the poorest CC performance in all conditions. Even though adverse atmospheric condition makes CC values for all frequencies much worse, the hierarchy of relative

performance remains broadly consistent. These results offer valuable insights for optimizing the design of communication systems based on the predicted atmospheric conditions and required reliability thresholds. As an example, subject to an acceptable BER (1e-09) and a Q factor (≈6), the estimated CCs required for each data transmission from the FSO BS to the UAVs are, in the LR case: 4.719e+10 bps at 1651 m (UAV1), 4.934e+10 bps at 1486 m (UAV2), 3.896e+10 bps at 1336 m (UAV3) and 5.321e+10 bps at 600 m (UAV4). Furthermore, in the MH case, the estimated CCs are, respectively, 5.092e+10 bps at 1763 m (UAV1), 5.201e+10 bps at 1587 m (UAV2), 5.167e+10 bps at 1497 m (UAV3), and 5.414e+10 bps at 610 m (UAV4). Finally, for the HR case, the estimated CCs are, respectively, 2.352e+10 bps at 892.7 m (UAV1), 3.770e+10 bps at 809 m (UAV2), 4.104e+10 bps at 787.3 m (UAV3), and 5.413e+10 bps at 540 m (UAV4).

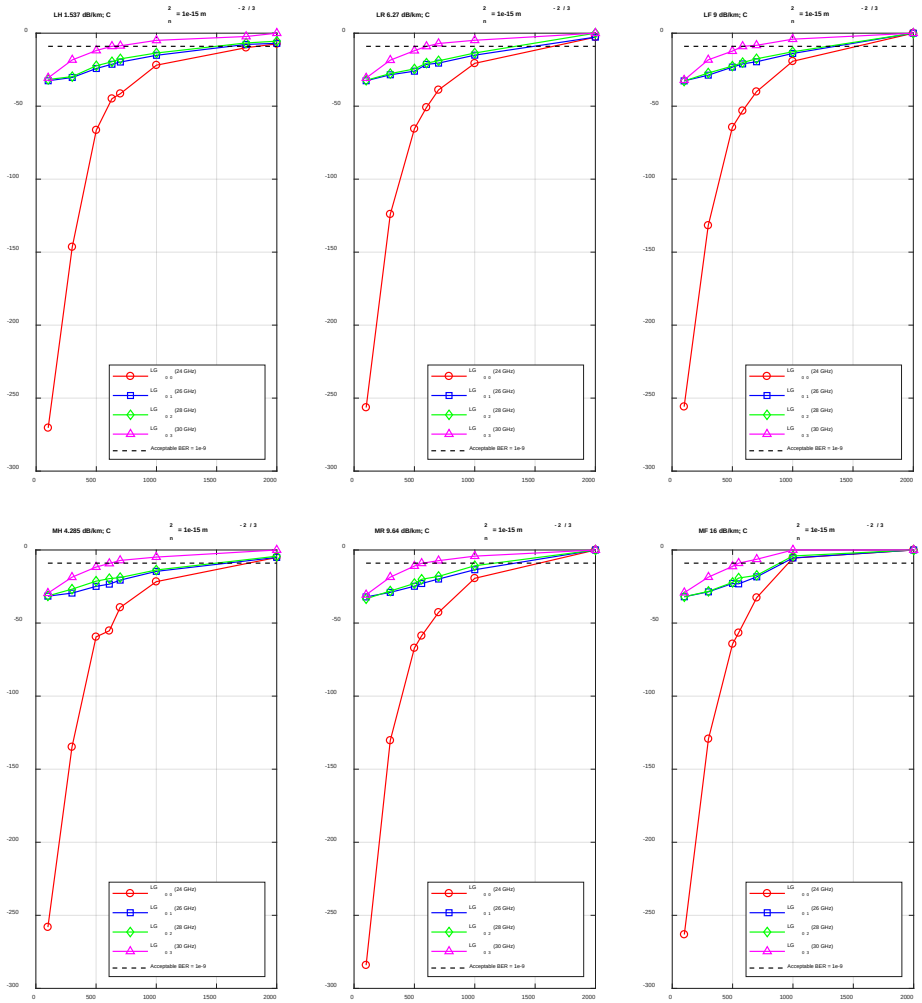

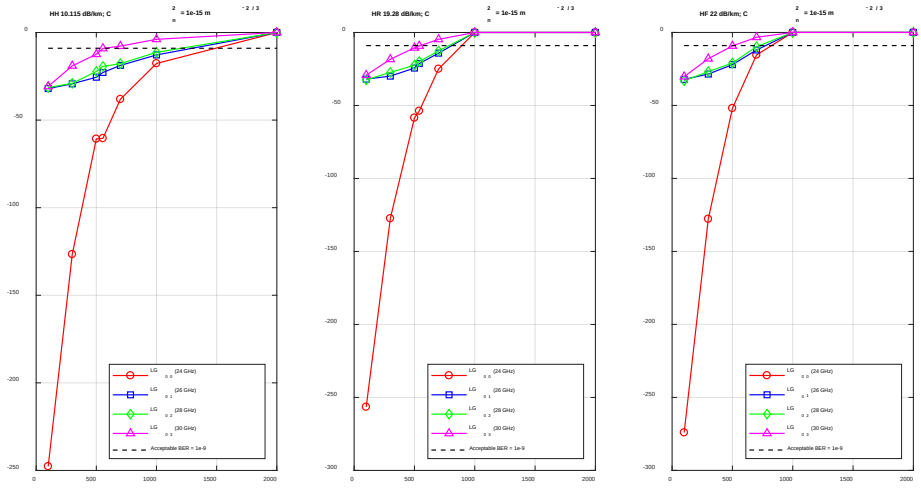

Figure 3.10. Min $\log_{10}$ BER vs. Distance of FSO link [m] under moderate AT.

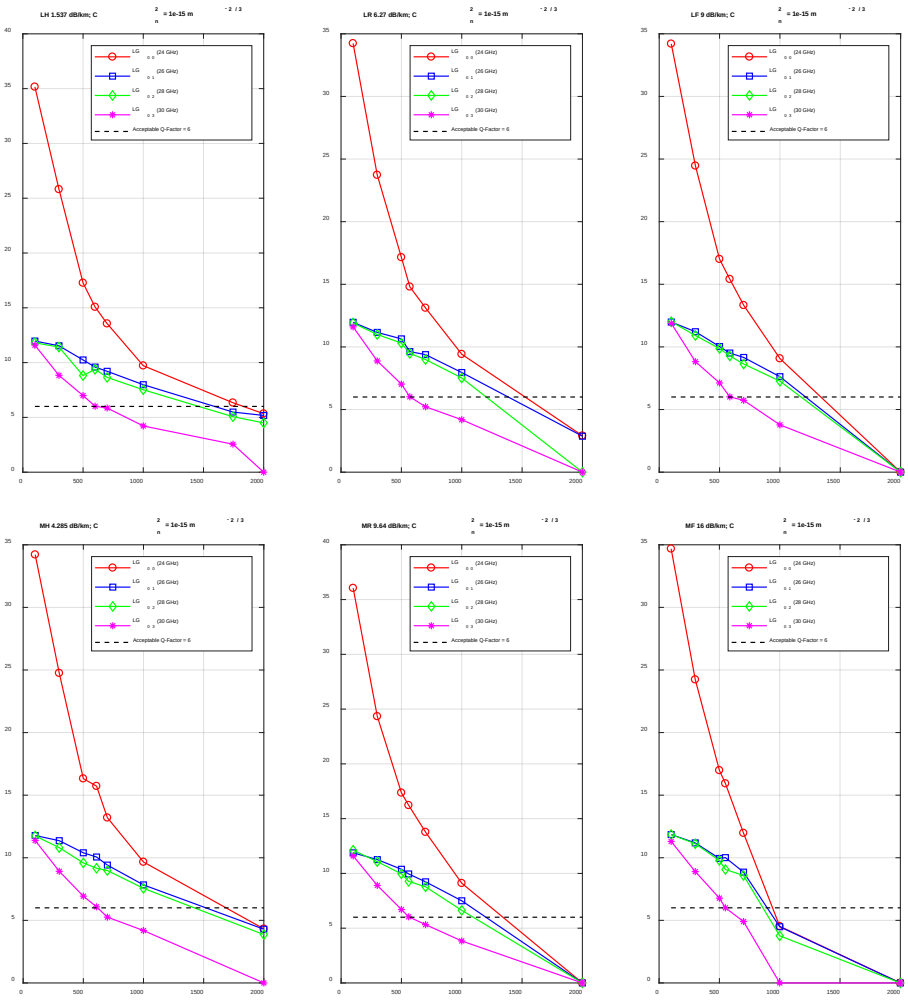

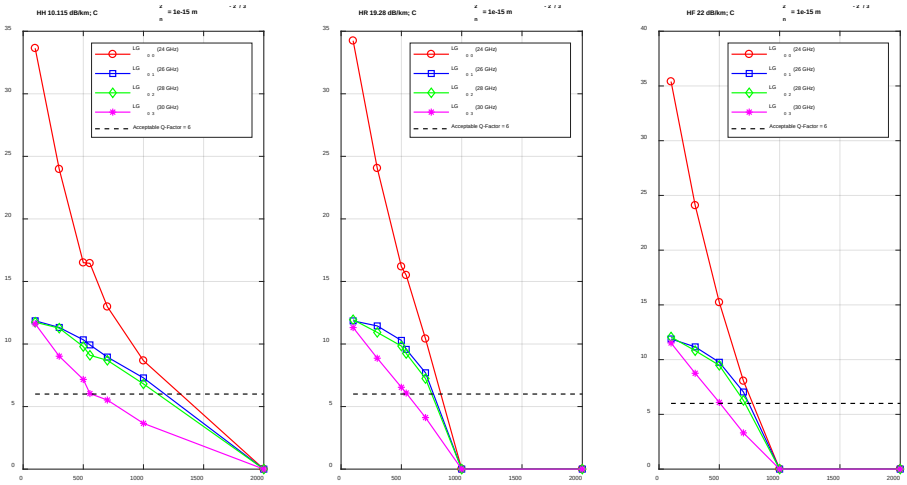

Figure 3.11. Q-Factor vs. Distance of FSO link [m] under moderate AT.

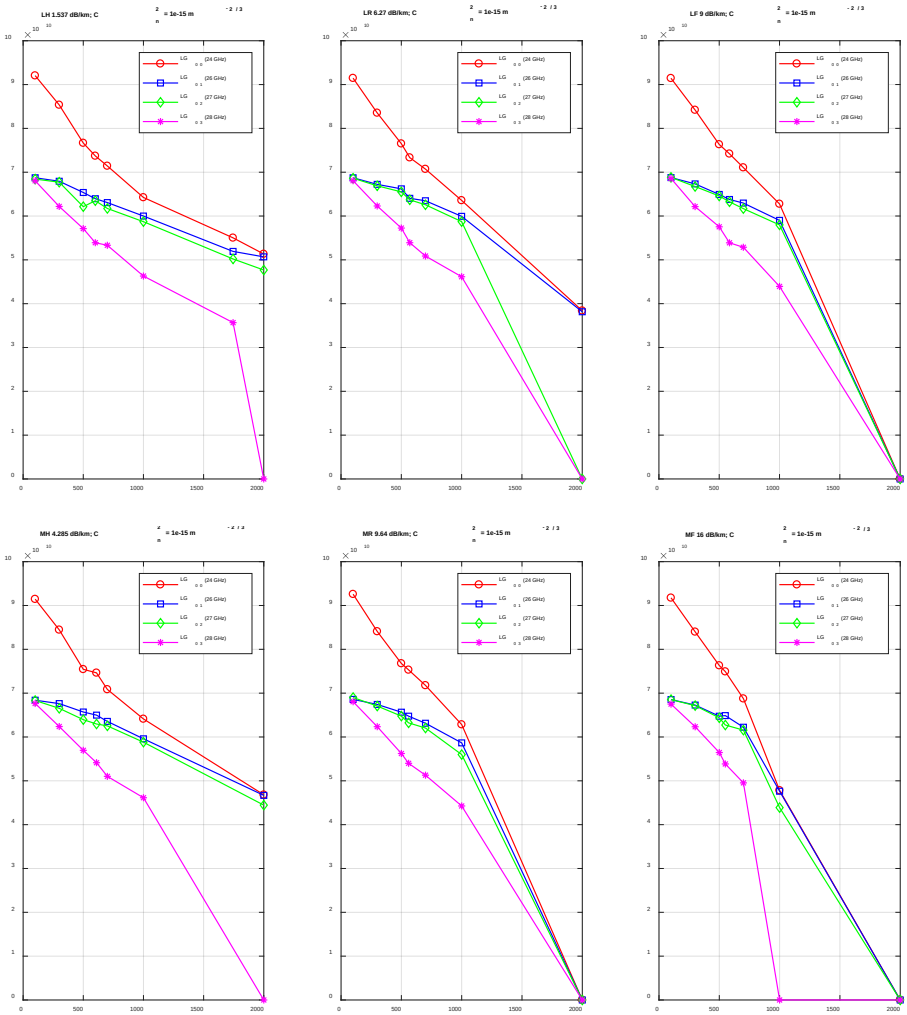

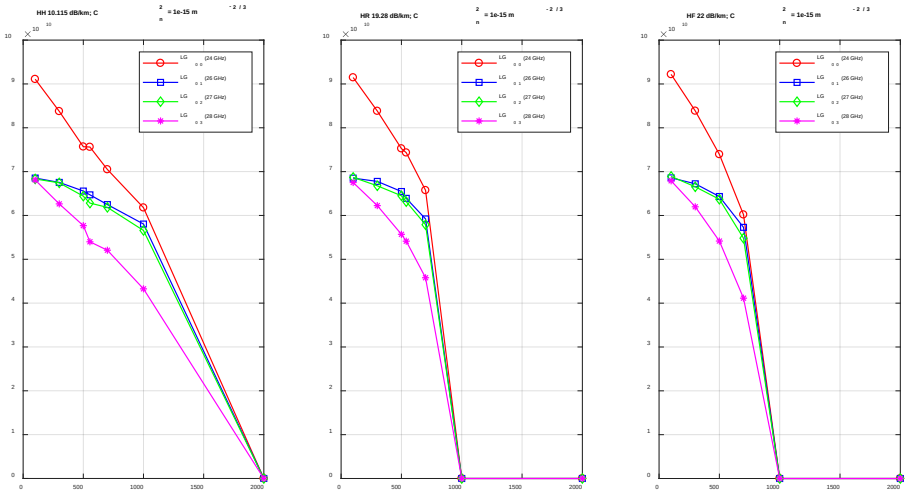

Figure 3.12. CC [bps] vs. Distance of FSO link [m] under moderate AT.

When there is strong turbulence, the BER (see Figure 3.13) curves show a significant degradation in performance as the transmission distance increases. However, the fundamental frequency of the LG_{00} mode (24 GHz for UAV1) exhibits a significantly lower BER than the obtained results in the first two scenarios, particularly under weak and moderate turbulence, and it varies slightly among the three levels of WCs, such as light, medium, and strong. In addition, the logarithmic scale of these graphs highlights the considerable increase in BER with distance in WCs. Finally, it is observed that the performance of the proposed system is limited to short communication distances of 5GBUN under strong turbulence for the four frequencies: 24 GHz (LG_{00} for UAV1), 26 GHz (LG_{01} for UAV2), 28 GHz (LG_{02} for UAV3), and 30 GHz (LG_{03} for UAV4), respectively.

Furthermore, the Q-Factor measurement (see Figure 3.14) shows a generally linear decrease (before the threshold line) in signal quality with increasing distance. Interestingly, the LG_{00} mode (24 GHz for UAV1) exhibits superior quality at short distances but deteriorates more rapidly as the distance between the FSO BS and the UAV1 node increases. Compared to the higher-order modes, the LG_{00} mode (24 GHz for UAV1) maintains signal integrity more effectively for short transmission distances, particularly when compared to the LG_{01} mode (26 GHz for UAV2), LG_{02} mode (28 GHz for UAV3), and LG_{03} mode (30 GHz for UAV4). The dashed threshold line (black legend) in these graphs represents the minimum acceptable quality level for reliable communication between each UAV node and the FSO BS.

For example, to obtain an acceptable BER (1e-09) and Q-Factor (≈ 6), the following distances are required for each UAV link in the LF case: 213.8 m (UAV1), 169.9 m (UAV2), 134.8 m (UAV3), and 47 m (UAV4). Furthermore, in the MF case, the following distances for

each UAV link are, respectively: 205.5 m (UAV1), 166.6 m (UAV2), 135 m (UAV3), and 46 m (UAV4). Finally, for the HH case, the following distances for each UAV link are, respectively: 218.4 m (UAV1), 144.1 m (UAV2), 136.6 m (UAV3), and 46.25 m (UAV4).

In contrast, the CC graphs (see Figure 3.15) exhibit a more unfavorable behavior, characterized by remarkable degradations that attest to the strong influence of turbulence. The fundamental LG_{00} mode (24 GHz for UAV1) generally maintains higher CC values over the entire transmission range than the higher-order modes, LG_{01} mode (26 GHz for UAV2), LG_{02} mode (28 GHz for UAV3), and LG_{03} mode (30 GHz for UAV4), although the degradation is more substantial in this range. In some cases, the LG_{01} (26 GHz for UAV2) and LG_{02} (28 GHz for UAV3) modes exhibit the same behavior; however, the LG_{03} mode (30 GHz for UAV4) performs less well under strong turbulence. As an example, subject to an acceptable BER (1e-09) and a Q factor (≈6), the estimated CCs required for each data transmission from the FSO BS to the UAVs are, in the LF case: 4.951e+10 bps at 213.8 m (UAV1), 5.19e+10 bps at 169.9 m (UAV2), 5.251e+10 bps at 134.8 m (UAV3) and 5.395e+10 bps at 47 m (UAV4). Furthermore, in the MF case, the estimated CCs are, respectively, 4.905e+10 bps at 205.5 m (UAV1), 5.158e+10 bps at 166.6 m (UAV2), 5.27e+10 bps at 135 m (UAV3), and 5.448e+10 bps at 46 m (UAV4). Finally, for the HH case, the estimated CCs are, respectively, 4.959e+10 bps at 218.4 m (UAV1), 5.233e+10 bps at 144.1 m (UAV2), 5.243e+10 bps at 136.6 m (UAV3), and 5.435e+10 bps at 46.25 m (UAV4).

In conclusion, based on the simulation results and performance analysis under various AT conditions, the 24 GHz (LG_{00} for UAV1) frequency was found to be the most reliable and consistent. In addition, it maintained a low BER, a high Q-Factor, and comparable CC in different WC scenarios and over various transmission distances. However, the higher frequencies, such as 26 GHz (LG_{01} for UAV2), 28 GHz (LG_{02} for UAV3), and 30 GHz (LG_{03} for UAV4), were more susceptible to atmospheric attenuation, resulting in degraded signal quality, especially in foggy and rainy conditions.

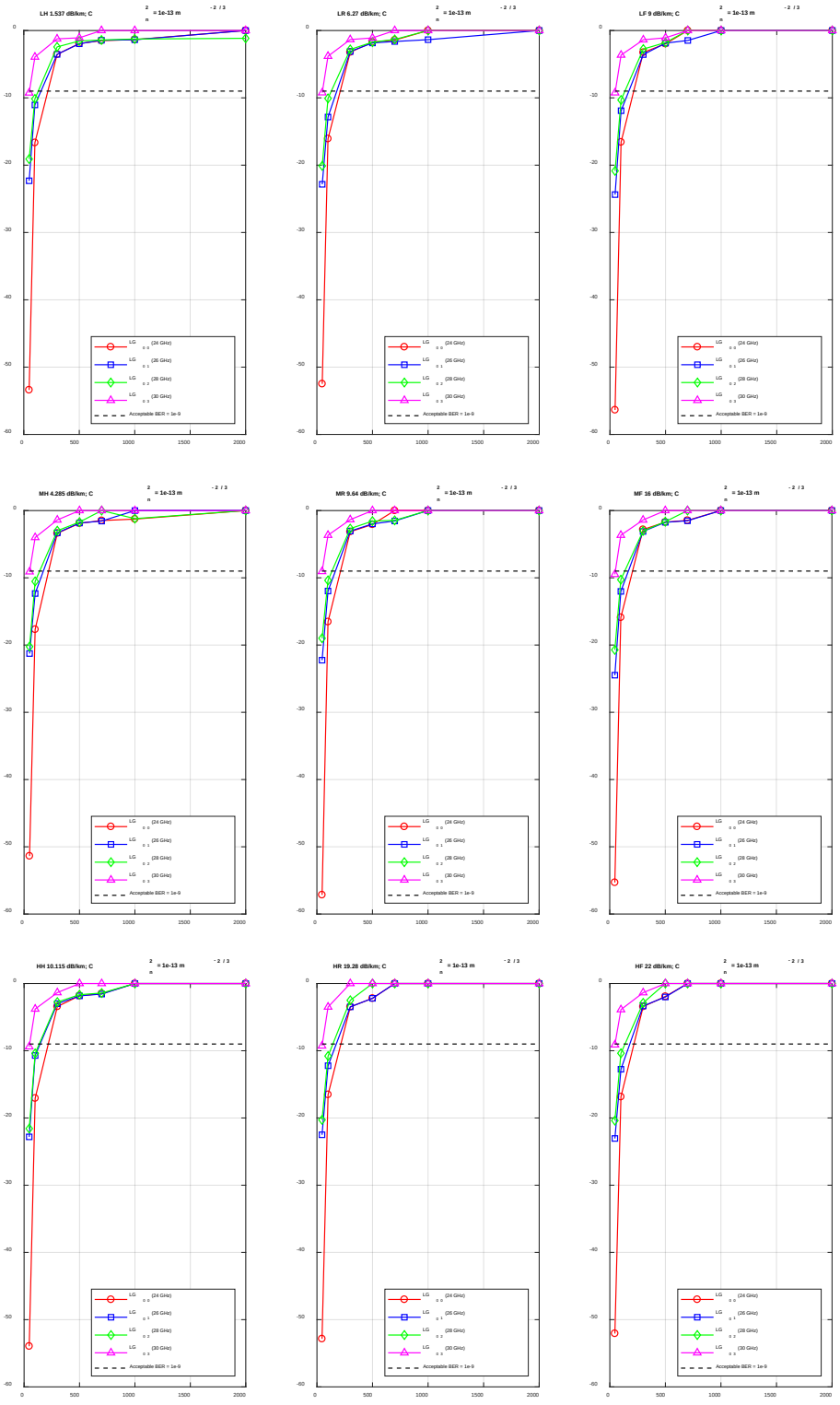

Figure 3.13. Min $\log_{10}$ BER vs. Distance of FSO link [m] under strong AT.

Finally, 24 GHz (LG_{00} for UAV1) is the most suitable frequency to ensure robust and high-quality RoMMF-FSO communication over long distances of a 5GBUN. For other frequencies, the application of a 5GBUN can be employed for short transmission distances.

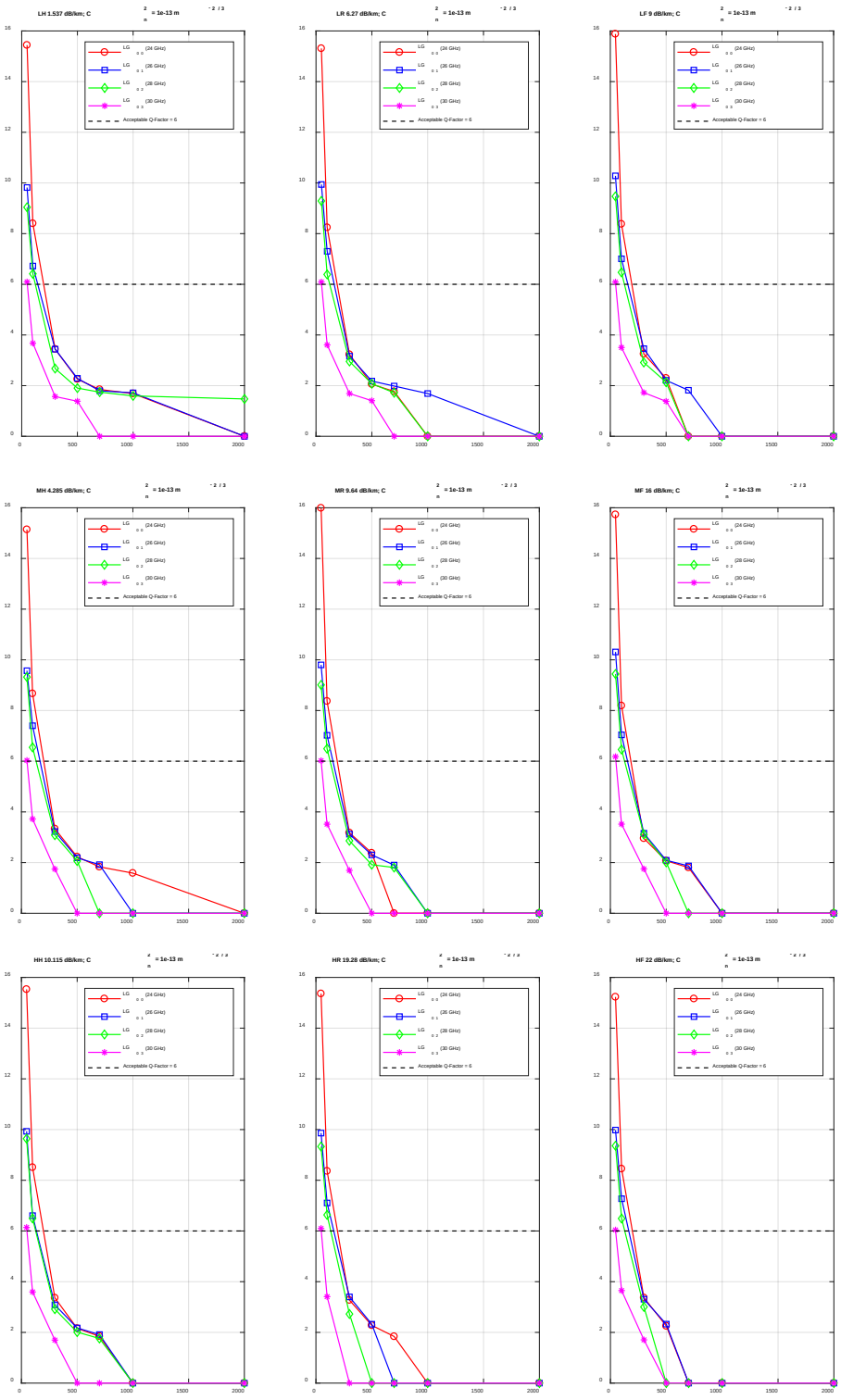

Figure 3.14. Q-Factor vs. Distance of FSO link [m] under strong AT.

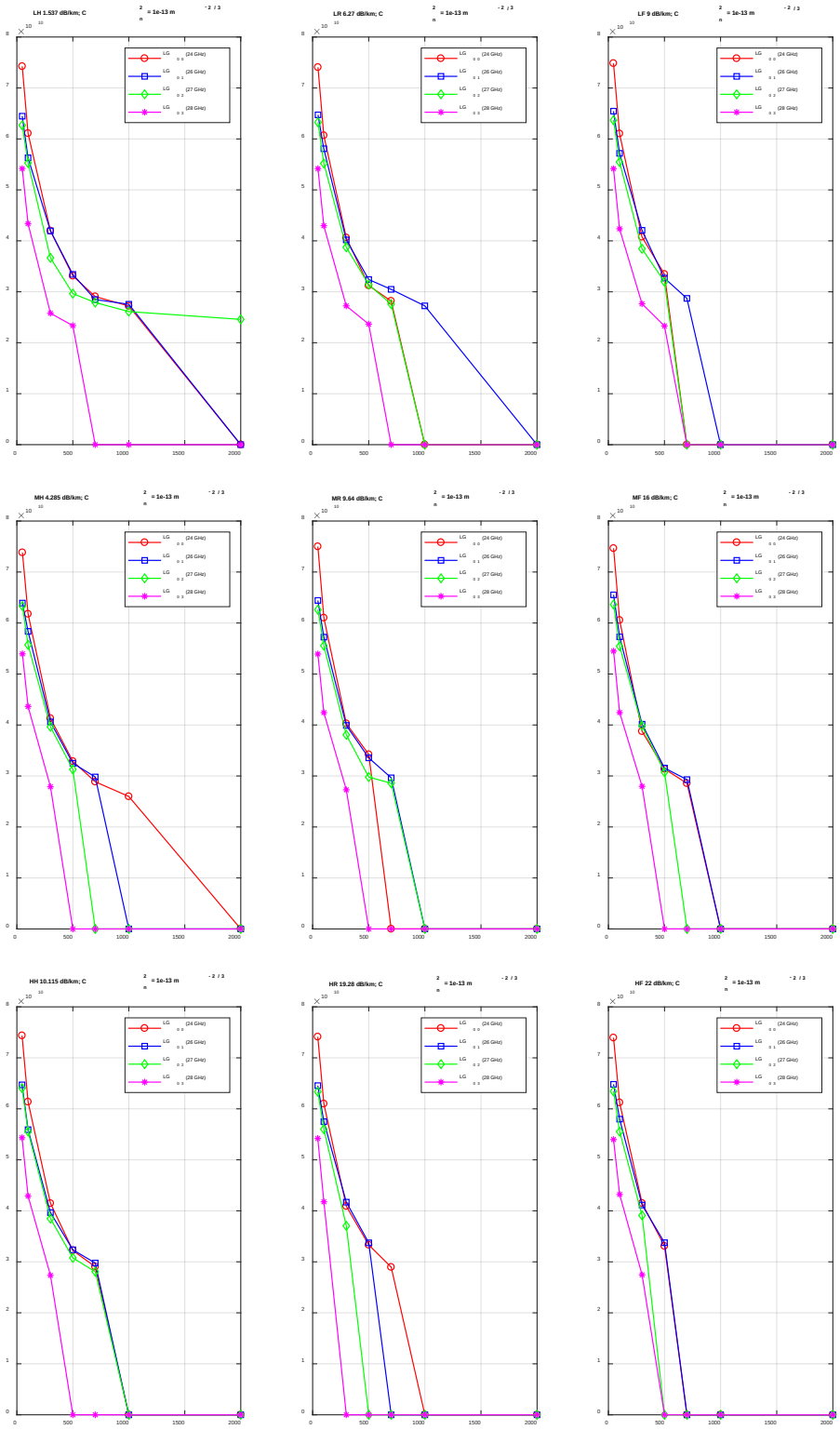

Figure 3.15. CC [bps] vs. Distance of FSO link [m] under strong AT.

3.5.2. Effects of transmission power (PTx) variation on the RoMMF-FSO link

It was observed that, in the case of weak AT (see Table 3.2), for the majority of WCs and distances considered, a transmission power of 10 dBm was sufficient on all tested frequencies [24 GHz (LG_{00} for UAV1), 26 GHz (LG_{01} for UAV2), 28 GHz (LG_{02} for UAV3) and 30 GHz (LG_{03} for UAV4)]. This result indicates optimal energy performance without additional power costs, which is very favorable from both operational and economic points of view for the proposed system.

However, under more demanding WCs, such as LF and MR (e.g., 9 dB/km or 9.64 dB/km) and longer target distances (e.g., 1395 m and 1343 m), higher frequencies such as 28 GHz (LG_{02} for UAV3) and 30 GHz (LG_{03} for UAV4) required notable power increases, reaching up to [+11.5 % to +52 %] power variation compared to the reference (10 dBm). This results in a significant energy cost, which reduces the overall system efficiency. Therefore, from an economic and energy efficiency point of view, the 24 GHz (LG_{00} for UAV1) and 26 GHz (LG_{01} for UAV2) frequencies are the most optimal, providing excellent performance while maintaining minimal power increases under adverse environmental conditions (LF and MR).

WCs	**Under weak AT (1e-17 $m^{-2/3}$)**	**24 GHz**	**26 GHz**	**28 GHz**	**30 GHz**
1.537 dB/km	Estimated max range for 10 dBm	3437 m	3306 m	3058 m	2409 m
	Estimated Ptx for 3437 m	10 dBm	10.7 dBm	11.25 dBm	15.5 dBm
6.27 dB/km	Estimated max range for 10 dBm	1746 m	1706 m	1634 m	1396 m
	Estimated Ptx for 1746 m	10 dBm	10.65 dBm	11.22 dBm	15.21 dBm
9 dB/km	Estimated max range for 10 dBm	1395 m	1359 m	1339 m	1088 m
	Estimated Ptx for 1395 m	10 dBm	10.6 dBm	11.15 dBm	15.1 dBm
4.285 dB/km	Estimated max range for 10 dBm	2115 m	2085 m	1978 m	1709 m
	Estimated Ptx for 2115 m	10 dBm	10.45 dBm	11.1 dBm	14.98 dBm
9.64 dB/km	Estimated max range for 10 dBm	1343 m	1319 m	1283 m	1049 m
	Estimated Ptx for 1343 m	10 dBm	10.50 dBm	11.35 dBm	15.19 dBm
16 dB/km	Estimated max range for 10 dBm	990.9 m	953.2 m	940.5 m	784.7 m
	Estimated Ptx for 990.9 m	10 dBm	11.21 dBm	12.1 dBm	15.7 dBm
10.115 dB/km	Estimated max range for 10 dBm	1305 m	1284 m	1240 m	1002 m
	Estimated Ptx for 1305 m	10 dBm	10.6 dBm	11.34 dBm	15.18 dBm
19.28 dB/km	Estimated max range for 10 dBm	857 m	842.7 m	812.3 m	681.7 m
	Estimated Ptx for 857 m	10 dBm	10.55 dBm	11.48 dBm	15.21 dBm
22 dB/km	Estimated max range for 10 dBm	780.4 m	762 m	744.4 m	641.5 m
	Estimated Ptx for 780.4 m	10 dBm	10.59 dBm	11.4 dBm	15.2 dBm

Table 3.2. Effect of PTx variation on the RoMMF-FSO link under weak AT.

However, under moderate (see Table 3.3) and strong (see Table 3.4) AT conditions, weather disturbances significantly degraded performance of the proposed system, making it impractical to maintain optimal distances across all frequencies, 24 GHz (LG_{00} for UAV1), 26 GHz (LG_{01} for UAV2), 28 GHz (LG_{02} for UAV3) and 30 GHz (LG_{03} for UAV4). Therefore,

the strategy was modified: the transmission distance was fixed based on the worst-case frequency of 30 GHz (LG_{03} for UAV4), and the transmitter power for each frequency was reduced just enough to maintain this shorter, unified distance. Finally, this approach is feasible due to the assumption of a mobile BS (UAV), such as a drone, which allows for flexible adjustment of the distance and avoids the limitations imposed by fixed-distance infrastructure.

WCs	**Under moderate AT (1e-15 $m^{-2/3}$)**	**24 GHz**	**26 GHz**	**28 GHz**	**30 GHz**
1.537 dB/km	Estimated max range for 10 dBm	1836 m	1613 m	1495 m	630 m
	Estimated Ptx for 630 m	-7.40 dBm	-6.80 dBm	-6 dBm	10 dBm
6.27 dB/km	Estimated max range for 10 dBm	1651 m	1486 m	1336 m	600 m
	Estimated Ptx for 600 m	-4.9 dBm	-4.2 dBm	-3.5 dBm	10 dBm
9 dB/km	Estimated max range for 10 dBm	1531 m	1346 m	1290 m	585 m
	Estimated Ptx for 585 m	-3.5 dBm	-2.7 dBm	-2 dBm	10 dBm
4.285 dB/km	Estimated max range for 10 dBm	1763 m	1587 m	1497 m	610 m
	Estimated Ptx for 610 m	-5.8 dBm	-5.2 dBm	-4 dBm	10 dBm
9.64 dB/km	Estimated max range for 10 dBm	1535 m	1333 m	1165 m	560 m
	Estimated Ptx for 560 m	-3.6 dBm	-3 dBm	-2.2 dBm	10 dBm
16 dB/km	Estimated max range for 10 dBm	962.3 m	915.9 m	887 m	550 m
	Estimated Ptx for 550 m	-0.5 dBm	0 dBm	1 dBm	10 dBm
10.115 dB/km	Estimated max range for 10 dBm	1493 m	1301 m	1201 m	555 m
	Estimated Ptx for 555 m	-3.5 dBm	-3.1 dBm	-2.1 dBm	10 dBm
19.28 dB/km	Estimated max range for 10 dBm	892.7 m	809 m	787.3 m	540 m
	Estimated Ptx for 540 m	1 dBm	1.6 dBm	2.6 dBm	10 dBm
22 dB/km	Estimated max range for 10 dBm	826 m	774.2 m	724.2 m	500 m
	Estimated Ptx for 500 m	1.2 dBm	1.8 dBm	2.7 dBm	10 dBm

Table 3.3. Effect of PTx variation on the RoMMF-FSO link under moderate AT.

WCs	**Under strong AT (1e-13 $m^{-2/3}$)**	**24 GHz**	**26 GHz**	**28 GHz**	**30 GHz**
1.537 dB/km	Estimated max range for 10 dBm	216.5 m	154.6 m	129.4 m	50 m
	Estimated Ptx for 50 m	-19.8 dBm	-19.3 dBm	-18 dBm	10 dBm
6.27 dB/km	Estimated max range for 10 dBm	210.1 m	179.1 m	129.7 m	49 m
	Estimated Ptx for 49 m	-19.75 dBm	-19.1 dBm	-18.1 dBm	10 dBm
9 dB/km	Estimated max range for 10 dBm	213.8 m	169.9 m	134.8 m	47 m
	Estimated Ptx for 47 m	-19.72 dBm	-19.08 dBm	-18.18 dBm	10 dBm
4.285 dB/km	Estimated max range for 10 dBm	220.6 m	172.5 m	139.8 m	49.5 m
	Estimated Ptx for 49.5 m	-19.7 dBm	-19.1 dBm	-18.15 dBm	10 dBm
9.64 dB/km	Estimated max range for 10 dBm	211.2 m	165.1 m	135.9 m	46.5 m
	Estimated Ptx for 46.5 m	-19.70 dBm	-19.07 dBm	-18.15 dBm	10 dBm
16 dB/km	Estimated max range for 10 dBm	205.5 m	166.6 m	135 m	46 m
	Estimated Ptx for 46 m	-19.6 dBm	-19.05 dBm	-18.16 dBm	10 dBm
10.115 dB/km	Estimated max range for 10 dBm	218.4 m	144.1 m	136.6 m	46.25 m
	Estimated Ptx for 46.25 m	-19.55 dBm	-19 dBm	-18.14 dBm	10 dBm
19.28 dB/km	Estimated max range for 10 dBm	215.2 m	173.7 m	143 m	45.75 m
	Estimated Ptx for 45.75 m	-19.4 dBm	-18.8 dBm	-18.135 dBm	10 dBm
22 dB/km	Estimated max range for 10 dBm	217.1 m	179.8 m	136.7 m	45.5 m
	Estimated Ptx for 45.5 m	-19.3 dBm	-18.5 dBm	-17.6 dBm	10 dBm

Table 3.4. Effect of PTx variation on the RoMMF-FSO link under strong AT.

3.5.3. Cost analysis based on AT conditions and deployment 5GBUN strategy

Table 3.5 summarizes some of the transmitter power requirements and their corresponding cost expressions (in units of x) in different AT scenarios: low, moderate, and strong for different WCs. The cost variation (x %) indicates the relative increase or decrease from the reference power of 10 dBm. For example, under weak AT conditions with LF scenario, power and thus cost increased significantly for higher frequencies, especially 30 GHz (+51%). In contrast, under moderate and strong AT scenarios, the required transmitter power was reduced for most frequencies due to shorter transmission distances, resulting in cost savings of up to 13% (e.g., at 24 GHz). These results demonstrate that power optimization under AT conditions can achieve both performance reliability and energy cost efficiency.

Scenario	**Frequency**	**WC/distance**	**Power**	**Cost expression**	**Cost variation (x %)**
Weak AT	24 GHz	LF/1395 m	10.00 dBm	10.00+x	+00.00 %
	26 GHz		10.60 dBm		+06.00 %
	28 GHz		11.15 dBm		+11.50 %
	30 GHz		15.10 dBm		+51.00 %
Moderate AT	24 GHz	HF/500 m	1.2 dBm		-88.00 %
	26 GHz		1.8 dBm		-82.00 %
	28 GHz		2.7 dBm		-73.00 %
	30 GHz		10.00 dBm		+00.00 %
Strong AT	24 GHz	MF/46 m	-19.6 dBm		-296.00 %
	26 GHz		-19.05 dBm		-290.50 %
	28 GHz		-18.16 dBm		-281.6 %
	30 GHz		10.00 dBm		+00.00 %

Table 3.5. PTx costs as a function of AT scenarios.

3.5.4. Comparative analysis of RoMMF-FSO performance on weak, moderate and strong ATs

When comparing the performance of RoMMF-FSO under weak, moderate, and strong AT conditions, several significant differences emerge in the behavior of BER, Q-Factor, and CC measurements of the proposed system (see Table 3.6). In conclusion, here are a few key points:

- Weak AT enables the RoMMF-FSO communication to perform optimally by providing superior signal quality, a low BER, and a high CC within a 5GBUN area.

- Moderate AT poses some problems, but the RoMMF-FSO communication still works well as long as power levels are reasonable within a 5GBUN area.
- Strong AT has a significant impact on performance, making the RoMMF-FSO communications less reliable and less efficient, even when the transmit power is high within a 5GBUN area.

AT types	**Weak (1e-17 $m^{-2/3}$)**	**Moderate (1e-15 $m^{-2/3}$)**	**Strong (1e-13 $m^{-2/3}$)**
BER	Very low BER, meaning minimal signal distortion and secure transmission.	Higher BER compared to low turbulence, but still possible with increased power for safe transmission.	A significantly large BER, especially at low power levels, indicates poor reliability.
Q-Factor	A high Q factor means that the signal quality is excellent and the noise level is very low.	The Q factor is attenuated, which reflects moderate signal degradation due to turbulence.	The behavior of the Q factor is particularly unfavorable in terms of noise and signal distortion due to turbulence.
CC	High and increasing CC with transmit power; excellent RoMFF-FSO channel efficiency.	CC effective, but at a slower rate than in weak turbulence.	CC is limited; atmospheric effects hinder system performance.

Table 3.6. Comparative analysis of the proposed system under different ATs.

3.6. Future works

Future research will focus on enhancing the resilience of the RoMMF-FSO link against challenging WCs, which have been demonstrated to have a considerable impact on its performance. In addition, adaptive modulation schemes and error correction techniques can be executed to support the communication quality of the RoMMF-FSO link under dynamic AT conditions. Furthermore, real-time weather monitoring and intelligent switching between the FSO communication system and other MMW channels can improve link reliability. Also, the use of lower frequency bands and shorter transmission ranges can reduce attenuation consequences. Ultimately, executing machine learning algorithms for predictive link

adaptation and testing the system in real outdoor environments will be indispensable for its practical deployment in 5G networks.

3.7. Conclusion

This study demonstrated the potential of the RoMMF-FSO link in the proposed system as a viable solution for high-speed 5G wireless communication, especially for a 5GBUN using UAVs. Simulation results under various AT conditions demonstrated that the system performs reliably in light and medium weather scenarios, with acceptable BER, Q-Factor, and CC values across all tested frequencies, 24 GHz, 26 GHz, 28 GHz, and 30 GHz. However, the proposed system's performance decreases significantly over long transmission distances and at higher frequencies, such as 28 GHz and 30 GHz, especially when there is considerable rain and fog. In addition, the RoMMF-FSO link remains a promising candidate for a 5GBUN, provided that the weather impact is carefully mitigated. Ultimately, these results highlight the importance of employing environmental adaptability and awareness strategies to ensure that all WCs operate optimally in real-world scenarios.

3.8. References of chapter 3

1. Jurado-Navas, A., Tatarczak, A., Lu, X., Olmos, J. J. V., Garrido-Balsells, J. M., & Monroy, I. T. (2015). 850-nm hybrid fiber/free-space optical communications using orbital angular momentum modes. Optics express, 23(26), 33721-33732.
2. Zeb, K. (2023). Quantum Dash Multi-Wavelength Lasers for Next Generation High Capacity Multi-Gb/s Millimeter-Wave Radio-over-Fiber Wireless Communication Networks (Doctoral dissertation, Concordia University).
3. Sood, A., & Kaushik, R. (2024). 4× 20 Gbps-60 GHz hybrid RoF-FSO transmission link for last mile connectivity. Journal of Optics, 53(2), 1095-1105.
4. Elsayed, E. E. (2024). Investigations on OFDM UAV-based free-space optical transmission system with scintillation mitigation for optical wireless communication-to-ground links in atmospheric turbulence. Optical and Quantum Electronics, 56(5), 837.
5. Shaker, F. K., Mohammed, F. S., & Khudhair, M. J. (2024). Atmosphere turbulence effects on a multiple apertures free space optical communication systems. Journal of Optical Communications.
6. Zitelli, M. (2025). A thermodynamic approach to linear and quantum cross-talk in multimode fiber systems. Journal of Lightwave Technology.

7. Rosales-Guzmán, C., & Forbes, A. (2024). Structured Light with Spatial Light Modulators. SPIE.
8. Zia, D., Zitelli, M., Carvacho, G., Spagnolo, N., Sciarrino, F., & Wabnitz, S. (2024). Modal division multiplexing of quantum and classical signals in few-mode fibers. arXiv preprint arXiv:2412.17578.
9. Xu, J., Huang, H. C., Wu, J., Cui, S., Liu, M., & Li, H. (2024). Integrated millimeter-wave and microwave antennas for mobile phones. IEEE Antennas and Wireless Propagation Letters.
10. Alanazi, M. D., Ali, W. A., Abdelhady, M. A., & Ibrahim, A. A. (2025). Millimeter-wave monopole antenna with circular polarization utilizing FSS polarizer for 5G communications. Engineering Science and Technology, an International Journal, 61, 101931.
11. Guo, W., Zhang, Z., Chang, L., Song, Y., & Yin, L. (2024). A ddos tracking scheme utilizing adaptive beam search with unmanned aerial vehicles in smart grid. Drones, 8(9), 437.
12. Khan, N., Ahmad, A., Wakeel, A., Kaleem, Z., Rashid, B., & Khalid, W. (2024). Efficient UAVs deployment and resource allocation in UAV-relay assisted public safety networks for video transmission. IEEE Access, 12, 4561-4574.
13. https://optiwave.com/optisystem-overview. Accessed 06/21/2025 at 23:38 p.m.
14. Kadhim, M., & Murdas, I. A. (2024, November). Performance Analysis of Optical Communication System Based on Ultra-high Capacity WDM-SDM Techniques. In 2024 3rd International Conference on Advances in Engineering Science and Technology (AEST) (pp. 166-171). IEEE.
15. Ejaz, S., Shafqat, S., Qureshi, K., Qamar, F., Shahzadi, R., & Ali, M. (2025). Performance comparison of Duobinary, AMI, CNRZ and CSRZ for next generation FSO communication system. Journal of Optical Communications, 45(s1), s2785-s2794.
16. Adardour, H. E. (2024). Advanced Optical-Radio Communication System for 5G Base Stations at 60 GHz Using MMW-FSO Links with Integrated Space-Division Multiplexing. Wireless Personal Communications, 1-75.
17. Magidi, S., & Pondani, T. (2025). Mode Division Multiplexing Free Space Optical Communication System Performance with Aperture Averaging in Atmospheric Turbulence and Various Weather Conditions. Engineering Innovations, 12, 65-76.
18. Magidi, S., & Pondani, T. (2020). Estimating the performance of free space optical communication in rain weather conditions using various models and modified duobinary

return to zero technique. Proceedings of the National Academy of Sciences, India Section A: Physical Sciences, 1-8.

19. Siegman, A. E. (1986). Lasers. University science books.
20. Ghatak, A. K., & Thyagarajan, K. (1998). An introduction to fiber optics. Cambridge university press.
21. Rashed, A. N. Z., Ahammad, S. H., Daher, M. G., Sorathiya, V., Siddique, A., Asaduzzaman, S., ... & Abdelhamid, H. S. (2025). Spatial single mode laser source interaction with measured pulse based parabolic index multimode fiber. Journal of Optical Communications, 45(s1), s465-s473.
22. Furuya, K., & Suematsu, Y. (1980). Random-bend loss in single-mode and parabolic-index multimode optical fiber cables. Applied optics, 19(9), 1493-1500.
23. Prabu, R. T., Sundar, S., Mary, M. L. L., Arumugam, A. R., Devi, P. K., Subha, T. D., & Anwer, K. T. (2025). High speed broadband light spatial laser system with hybrid linear/parabolic/measured indexed multimode optical fibers performance signature. Journal of Optical Communications, 45(s1), s2825-s2834.
24. Modalavalasa, S. K., Miglani, R., Chaudhary, S., Tubbal, F., & Raad, R. (2021). Developing cost-effective and high-speed 40 Gbps FSO systems incorporating wavelength and spatial diversity techniques. Frontiers in Physics, 9, 744160.
25. Amphawan, A., Chaudhary, S., Ghassemlooy, Z., & Neo, T. K. (2020). 2× 2-channel mode-wavelength division multiplexing in Ro-FSO system with PCF mode group demultiplexers and equalizers. Optics Communications, 467, 125539.
26. Singh, M., Atieh, A., Aly, M. H., & Abd El-Mottaleb, S. A. (2022). 120 Gbps SAC-OCDMA-OAM-based FSO transmission system: Performance evaluation under different weather conditions. Alexandria Engineering Journal, 61(12), 10407-10418.
27. Singh, M., Pottoo, S. N., Armghan, A., Aliqab, K., Alsharari, M., & Abd El-Mottaleb, S. A. (2022). 6G network architecture using FSO-PDM/PV-OCDMA system with weather performance analysis. Applied Sciences, 12(22), 11374.
28. Anuar, M. S., AlJunid, S. A., Arief, A. R., Junita, M. N., & Saad, N. M. (2013). PIN versus Avalanche photodiode gain optimization in zero cross correlation optical code division multiple access system. Optik, 124(4), 371-375.
29. Ahmed, H. Y., Zeghid, M., Bouallegue, B., Chehri, A., & Abd El-Mottaleb, S. A. (2022). Reduction of complexity design of SAC OCDMA systems by utilizing diagonal permutation shift (DPS) codes with single photodiode (SPD) detection technique. Electronics, 11(8), 1224.

30. Bouanane, L., Abbou, F. M., Abdi, F., Chaatit, F., & Abid, A. (2018, October). The effect of weak atmospheric turbulence and fog on OOK-FSO communication system. In The Proceedings of the Third International Conference on Smart City Applications (pp. 144-150). Cham: Springer International Publishing.
31. Singh, M., Atieh, A., & Kakati, D. (2023). 200 Gbps free-space optics data transmission using orbital angular momentum multiplexed beams and PAM-4 signals. Optical and Quantum Electronics, 55(1), 24.
32. Adardour, H. E. (2023). Novel networks architecture using CWDM/DWDM/5G mmWave system over FSOC channel with RISP performance analysis. Optical and Quantum Electronics, 55(8), 752.

General conclusion

In this study, the performance of a RoMMF-FSO system under various atmospheric conditions, as simulated using OptiSystem software, has been examined for a 5GBUN. However, the tests and analysis focused on understanding how adverse weather phenomena, such as fog, rain, and haze, affect the performance of FSO links due to the high attenuation levels they introduce. In addition, through multiple simulation scenarios, we evaluated key performance metrics, including BER, Q-factor, and CC, for a range of transmission distances of the FSO link and selected transmit power levels at DTNCC.

The results demonstrate that Weather Conditions (WCs) have a significant impact on overall system performance. However, the use of multi-beam MMW signal transmission in the RoMMF-FSO configuration improved system robustness by compensating for signal degradation in the FSO channel. Also, increasing the transmit power at the DTNCC helped improve signal quality, but each type of weather caused its own problems that required careful calibration of parameters and system optimization.

The future research goal should be to improve the resilience of systems in severe WCs. For illustration, robust error correction algorithms and adaptive modulation techniques can be employed to ensure that performance remains constant even when WCs change. Also, the integration of real-time WCs monitoring and intelligent switching between FSO communication links and alternative RF communication links could further enhance link availability. In addition, the application of shorter transmission distances and lower frequencies within MMW bands will contribute to reducing signal loss in the atmosphere. Finally, developing machine learning algorithms for predictive link adaptation and validating system performance in real-world outdoor environments is essential for the successful application of next-generation 5G networks, in general, and 5GBUN networks, in particular.